Journal of
Medicinal Chemistry

Article

Chemoreactive-inspired discovery of influenza A virus dual inhibitor to block hemagglutinin-mediated adsorption and membrane fusion

Guangwei Wu, Guihong Yu, Yunjia Yu, Shuang Yang, Zhongwei Duan, Wei Wang, Yan-Kai Liu, Rilei Yu, Jing Li, Tianjiao Zhu, Qianqun Gu, and Dehai Li

J. Med. Chem., **Just Accepted Manuscript** • DOI: 10.1021/acs.jmedchem.0c00312 • Publication Date (Web): 10 Jun 2020

Just Accepted

is published by the American Chemical Society. 1155 Sixteenth Street N.W., Washington, DC 20036

Chemoreactive-inspired discovery of influenza A virus dual inhibitor to block hemagglutinin-mediated adsorption and membrane fusion

Guangwei Wu,[†,#] Guihong Yu,[†,#] Yunjia Yu,[†,#] Shuang Yang,[†,#] Zhongwei Duan,[†] Wei Wang, [†,‡,*] Yankai Liu,[†] Rilei Yu,[†] Jing Li,[†] Tianjiao Zhu,[†] Qianqun Gu,[†] Dehai Li,[†,‡,*]

[†]Key Laboratory of Marine Drugs, Chinese Ministry of Education; School of Medicine and Pharmacy, Ocean University of China, 5 Yushan Road, Qingdao, Shandong, P. R. China, 26003.

[‡]Laboratory for Marine Drugs and Bioproducts, Pilot National Laboratory for Marine Science and Technology, Qingdao, People's Republic of China, 266200.

Abstract

Owing to the emergence of drug resistance, high morbidity and mortality, the need for novel anti-Influenza A virus (IAV) drugs with divergent targets is highly sought. Herein, we reveal the discovery of an anti-IAV agent as dual inhibitor to block hemagglutinin-mediated adsorption and membrane fusion by using a chemoreactive *ortho*-Quinone methide (*o*-QM) equivalent. Based on the *o*-QM equivalent non-enzymatically multipotent behavior, we created a series of clavatol-derived pseudo natural products and found that penindolone (PND), a new diclavatol indole adduct, exhibited potent and broad-spectrum anti-IAV activities with low risk of inducing drug resistance. Distinct from current anti-IAV drugs, PND possesses a novel scaffold, and is the first IAV inhibitor of targeting both HA1 and HA2 subunits of virus hemagglutinin to dually block IAV adsorption and membrane fusion process. More importantly, intranasal and oral administration of PND can protect mice against IAV-induced death and weight loss, superior to the effects of the clinical drug oseltamivir. Thus, the use of chemoreactive intermediates could expand our understanding of chemical diversity and aid in development of anti-IAV drugs with novel targets.

INTRODUCTION

Influenza A virus (IAV) is highly contagious respiratory pathogen and the main cause of seasonal and pandemic flu. Official WHO (World Health Organization) statistics indicate that the seasonal flu can cause serious infections in 3–5 million individuals, resulting in about 290,000 to 650,000 deaths per year worldwide.[1] In late April 2009, a novel influenza A (H1N1) virus caused a pandemic within a short period of time and attracted great attention all over the world.[2] To withstand influenza outbreaks in their early stages, small molecule drugs are usually one of the most effective and often first line of protection.[3] However, in the past few decades only six small molecule drugs, acting as ion channel blockers (amantadine and rimantadine), neuraminidase inhibitors (oseltamivir, zanamivir and peramivir) or polymerase inhibitors (baloxavir), were approved for commercial use by the U.S. FDA.[4] Despite these successes, drug resistance, toxicity, and cost remain unresolved issues in the fight against IAV infection.[5,6] Thus, therapeutics with novel mechanisms of action are urgently required to ease the persistent global threat imposed by influenza virus.

Natural products are essential for the discovery of novel drug leads and scaffolds.[7] With increasing knowledge of biosynthetic assembly pipelines, construction of natural products involve multiple building blocks coded by isolated gene clusters or even those producing from different organisms. Sometimes, these building blocks possess highly reactive and non-enzymatically susceptible moieties. After offloading from their designated biosynthetic machinery, these building blocks are stored in the same pool and could recognize each other based on non-enzymatic chemical coupling, a very energy-efficient strategy in nature to assemble functional molecules. Until now, most of

actual biological functions of these reactive building blocks and why they assemble together is less well known. However, it is clear that microorganisms have employed this strategy and preferential non-enzymatic chemical coupling to give a chemical arsenal to act as antibiotics and antidotes.[8-10] Such combined natural products seem to not only bring new insight to the assembly of natural products but also expand chemical space along with promising and diverse bioactivities, such as the migration inhibitor discoipyrroles and the new antibiotic malleonitrone.[8,11] Although there has been a sharp decrease in the direct use of natural products as approved drugs, natural product-derived pharmacophores still play predominant roles in drug development. Inspired by this, the application of chemoreactive building blocks toward the design of novel chemical entities may be useful in drug discovery programs.

ortho-Quinone methides (*o*-QMs), and their latent equivalents are well known to be highly reactive and useful intermediates as michael acceptors that can modify proteins to interfere with protein function. *o*-QMs have demonstrated widespread utility in the development of synthetic methodology and/or total syntheses of natural products,[12-14] and as well as the modification of some natural products scaffolds. Besides, they also serve as a chemical weapon for defense in a variety of plants, animals, and insects,[15] and can influence biologically active factors, such as vitamins E and K and the anthracycline antibiotics.[12] Overall, it still need further studies to understand and explore new functions of *o*-QMs. Clavatol is a small fungal polyketide with a range of biological activities.[16,17] Recent biosynthetic study suggested that clavatol is invovled in formation of penilactones and meanwhile, is found to be potential *o*-QMs behavior. Thus clavatol

could be excellent lead substrate for exploring the ability to create chemical diversity of pseudo natural products and discovering new bioactive small molecules.

With the clavatol producer (*Penicillum. crustosum* PRB-2) in hand,[18] we mimic the biosynthesis of penilactiones and create clavatol-derived pseudo natural products by aid of *o*-QM chemoreactive behavior and non-enzymatic chemical coupling, as well as chemical synthesis. As a promising result, penindolone (PND, **2**),[19.20] a new diclavatol indole adduct was found to display broad-spectrum anti-IAV activities with low risk of inducing drug resistance *in vitro*. Intranasal and oral administration of PND can protect mice against both IAV-induced death and weight loss, superior to the effects of the clinical drug oseltamivir. PND was further revealed to interact with two threonine residues in both HA1 and HA2 subunits of hemagglutinin (HA) and dually inhibit HA-mediated membrane fusion and virus entry process verified by hemagglutination inhibition (HI) and HA syncytium assays and H5N1 pseudovirus (H5N1-GFP) model studies. Herein, we report the discovery of PND, the *in vitro* and *in vivo* anti-IAV activities, pharmacokinetic profiles and dual inhibition mechanism for HA protein.

RESULTS AND DISCUSSION

New clavatol-oriented pseudo natural products produced by non-enzymatic chemical couplings

The *o*-QM form of clavatol displays electrophilic property and in an aqueous system is an equivalent of hydroxyclavatol.[21] Due to unstable feature of *o*-QM form of clavatol, pharmacological small molecules including eight indole-containing pharmacophores molecules (**i**–**viii**) and three aniline analogues (**ix**–**xi**) (Figure 1A), were selected and

incubated with the fungus *P. crustosum* PRB-2. Unexpectedly, supplementation with indole (**i**), indole-3-carboxaldehyde (**ii**) and indole-3-carboxylic acid (**iii**) resulted in the generation of monoclavatol- and biclavatol-based indole alkaloids **1** and **2** (Figure 1B and S1-S5, and Tables S1 and S2), while incubation with 2-phenylindole (**iv**) and 3,5-di(trifluoromethyl)aniline (**ix**) led to monoclavatol adducts **3** and **4**, respectively (Figures 1B, S2, S6, S7, and Tables S2 and S3). However, addition of 3-acetylindole (**v**), aniline derivatives **x** and **xi** did not result in any new products, and the media containing 2-methylindole (**vi**) 4-bromoindole (**vii**), and 5-methylindole (**viii**) were toxic to *P. crustosum,* preventing formation of downstream compounds. It is worth noting that **4** is unstable and transforms spontaneously to **ix** and a clavatol intermediate under mild conditions. Subsequent *in vitro* testing provided a proof of production of **1**–**4** via a non-enzymatic 1,4-Michael addition (Figures S8-14).

Biological evaluation of compounds 1-4

To discover novel chemotype inhibitors of influenza A virus, we first explored the anti-IAV effects of compounds **1**–**4** using the cytopathic effect (CPE) inhibition assay in PR8 infected MDCK cells. Compound **2**, harboring two clavatol moieties at the C-2 and C-3 positions on indole, exhibited the potent activity with IC_{50} of 12.5 μg/ml (26.4 μM), superior to the effects of ribavirin (98.3 μM), arbidol (32.5 μM), and the clinical drug oseltamivir (46.1 μM) (Table S6). The promising activity motivated us to yield more analogues to study structure-activity relationship and chemical diversity towards finding agents with increased anti-IAV activity.

Generation of diverse clavatol-oriented alkaloids by chemical synthesis

Intrigued by the promising ani-IAV activity of compound **2** and the potential utility of the *o*-QM form of clavatol, we synthesized more clavatol-containing derivatives of **2** and increase chemical diversity. It is obvious that chemical synthesis can bypass the induced toxicity affiliated with the indole precursors and accumulate efficient amounts of material for *in vivo* activity evaluations. The alternative *o*-QM form of clavatol (**xii**) is a suitable starting material for chemical diversification. Incubation of **i**, **iv**, **vii**, **viii**, **ix** and **xi** with **xii** in dioxane at 110 ^{o}C for 3 h yielded 11 additional clavatol-containing alkaloids (**5**–**15**), including **1**–**4** (Figure 1C and S1 and S2, and Tables S2, S4 and S5). Adducts **5**–**15** are new indole-clavatol alkaloids incorporating, to varying degrees, calvatol moieties at diverse reaction positions.

Evaluation of inhibition of influenza A virus of compounds 5-15 and cytotoxicity of 1-15

Synthetic compounds **5**–**15** were evaluated for inhibition of influenza A virus using the CPE inhibition assay in PR8 infected MDCK cells. Among them, compound **12**, structurally similar to compound **2**, which harbors two clavatol moieties at the C-2 and C-3 position on 4-methylindole exhibited the parallel anti-IAV activity with compound **2** (39.8 μM for **12** vs 26.4 μM for **2**, Table S6). The above results provided insight into the structure-activity relationship (SAR) that the incorporated number and position of clavatol moieties, and substituent groups on the indole were crucial for the anti-IAV activities. Althouth compounds **2** and **12** were weakly cytotoxic (CC_{50} > 10 μM) to some cancer cells, neither **2** nor **12** had obvious cytotoxicity against MDCK cells with CC_{50} values of 1472.0 μM and 680.7 μM, respectively (Table S6). The selectivity index (SI = CC_{50}/IC_{50}) of **2** (SI = 55.8) was superior to those of ribavirin (SI = 20.8), arbidol (SI =

10.4), and compound **12** (SI = 17.1). Compound **2**, named as penindolone (PND), was chosen to be further pharmacological investigated (Figure 2A and Table S6).

PND displays broad-spectrum anti-IAV activities with low risk of inducing drug resistance

To explore whether PND exerts broad antiviral spectrum activity, the inhibition by PND on virus titers from MDCK cells infected with PR8, H1N1 (A/California/04/2009) (Cal09) and H3N2 (A/swine/Minnesota/02719/2009) (Minnesota) at high moi (≈ 3.0 PFU/cell) were determined using the HA assay.[22-26] The results indicated that PND significantly inhibited the virus titers in PR8, Cal09 and Minnesota infected cells in a dose-dependent manner, with IC_{50} values < 10.0 *μ*g/ml, which was superior to the effects of arbidol and amantadine (Figure 2C and Table S7). Moreover, PND also significantly inhibited plaque formation in PR8, Cal09, Minnesota, Virginia/ATCC1/2009, and Aichi/2/1968 infected MDCK cells with IC_{50} values < 13.0 *μ*g/ml (Figure 2D and Figure S15 and Table S7), suggesting that PND possesses broad-spectrum anti-IAV activities i*n vitro*. Pre-treatment of IAV with PND in a dose-dependent manner reduced the formation of plaques in MDCK cells (Figure 2B), suggesting that PND may be able to inactivate viral particles directly.

To further explore whether PND induces drug resistance in IAV, a multi-passage experiment based on the CPE inhibition assay was performed.[27] A remarkable viral resistance was induced by amantadine (25 *μ*g/ml), suggesting that a low-level replication gives the IAV a chance to adapt to the selective pressure of amantadine within four passages (Figure 2E). However, PND could still significantly reduce the virus titer and promote cell viability after the fourth and fifth passage, suggesting that PND

was still efficient in inhibiting PR8 virus propagation (Figures 2E and F). Thus, PND possesses broad-spectrum anti-IAV activities with low risk of inducing drug resistance.

Intranasal or oral efficacy of PND against influenza infection *in vivo*

In line with its *in vitro* anti-IAV activity, intranasal or oral administration of PND protected mice against IAV-induced death and weight loss. Intranasal (20 or 40 μg/day) or oral (5 or 10 mg/kg/day) treatment of PND, initiated four hours after challenge and continuing for four days, resulted in significant decrease of pulmonary viral titers in comparison to the non-treated virus control group ($p < 0.05$) (Figure 3A and Table S8). Intranasal administration with PND (40 μg/day) resulted in 100% survival at day 14 in comparison to the oseltamivir (10 mg/kg/day) treated mice (80%) (Figure 3B and Table S8). In addition, the weights of the mice in the virus control group (Placebo) began to decrease at four days p.i., losing up to 23–24% of initial weight, before gradually recovering. In contrast, the PND treated mice gradually increased their body weights without weight loss (Figure 3C).

To assess the influence of PND on inflammatory symptoms in IAV infected mice, ELISA assays were performed to detect the production of cytokine TNF-α and IL-6 in lung tissues. As shown in Figure 3D, after intranasal or oral administration of PND for four days, TNF-α and IL-6 levels decreased significantly compared to that in the virus control group ($p < 0.05$) (Figure 3D). Histopathological analysis also showed that after intranasal or oral treatment of PND for four days, the IAV infected mice had intact columnar epithelia in the bronchiole without obvious inflammatory cell infiltration (Figure S16), comparable to the effect of oseltamivir (10 mg/kg/day). Thus, PND also possessed anti-IAV activities *in vivo.*

PND is orally bioavailable in mice and rats

The pharmacokinetic characteristics of PND were further investigated in mice (used for efficacy studies) and rats. PND could be detected within 5 min both in mice and rat plasma after single oral dosing, revealing quick absorption (Figure S17). The elimination half-life ($t_{1/2}$) of PND after intravenous administration was 3.4 h in mice and 4.8 h in rats. However, PND exposure *in vivo* was at low level with the oral bioavailability of 5.7% in mice and 1.4% in rats. Moreover, the renal excretion of prototype was less than 1% and the total recovery from urine and feces was no more than 30% 72 hours after intravenous administration in rodents, which revealed that PND might be biotransformed. We also observed that the values of C_{max} /dose and $AUC_{(0-t)}$ /dose, as well as the 72 hours cumulative excretion percentage in urine and feces were largely different between mice and rats. The significant species differences were also indicated by the different metabolic rate of PND in liver microsomes (Table 1). The NADPH-dependent degradation in human liver microsome was much less than that in mice/rat liver microsomes (Figure S18).

The toxicity effects to liver, kidney and heart of PND were preliminarily evaluated in mice. After treatment at 5 or 10 mg/kg of body weight once a day for 7 consecutive days, the representative biochemical parameters in serum including aspartate aminotransferase (AST), alanine aminotransferase (ALT), creatinine (CR), blood urea nitrogen (BUN), lactate dehydrogenase (LDH), creatine kinase (CK) and creatine kinase MB isoenzyme (CK-MB) have no siginificant change (Table S9). Thus, PND is not toxic to liver, kidney and heart.

PND blocks IAV infection through direct interaction with virus HA protein

The time-of-addition assay was performed to determine the stage(s) at which PND exerted its inhibitory activities *in vitro*. Addition of PND during adsorption or pretreatment of virus significantly decreased viral titers ($p < 0.01$), suggesting that PND inactivates viral particles directly to block the adsorption of IAV (Figure 4A). Thus, we first explored whether PND interacted with the virus surface NA protein by using the NA inhibition assay.[28] The results showed that PND did not significantly inhibit the activity of NA protein (Inhibition percentage < 15%) at the concentrations of 12.5-200 μg/ml, suggesting that NA protein is not the target of PND (Figure 4B).

The interaction between PND and viral HA protein was then evaluated using the hemagglutination inhibition (HI) and HA syncytium assays.[29,30] The results showed that PND significantly inhibited IAV-induced aggregation of red blood cell (RBC) at concentrations of 3.125-50 μg/mL (Figure 4C), suggesting that PND has a direct interaction with the HA protein. Moreover, overexpression of HA protein in Vero cells leads to significant syncytium formation upon lowering the pH from 7.0 to 5.0 without compound treatment (Figure 4D). PND (50 μg/ml) treatment significantly inhibited the HA syncytium formation in Vero cells (Figure 4D), suggesting that PND can block HA mediated membrane fusion.

Furthermore, the H5N1 pseudovirus (H5N1-Luc) model was used to further investigate the interaction of PND with IAV particles. The results indicate that PND (50 μg/ml) treatment dose-dependently blocked H5N1-Luc pseudovirus infection in MDCK cells ($P < 0.05$) (Figure 5A), and pretreatment of virus significantly decreased the amount of infected H5N1-Luc pseudovirus ($p < 0.01$), suggesting that PND may directly interact with virus HA protein (Figure 5B).

To further assess the interaction between PND and HA, the SPR assay was performed with different virus HA proteins. As shown in Figure 5C, the SPR data revealed a marked binding of PND to H1N1/PR8 HA with the KD equivalent to about 6.8 μM, implicating a high affinity of PND for HA protein. However, there was nearly no binding of PR8 HA protein to compound **1** which is a lack of clavatol group at C-2, suggesting that clavatol modification at C-2 is indispensible for the interaction of PND to HA protein (Figure 5D). Moreover, the direct binding of PR8 HA protein to salic acid analogue 3′-Sialyllactose (3′-SL) and the positive control arbidol was also evaluated by SPR assay and the interactions were observed with KD values of 4.5 μM and 11.1 μM, respectively (Figure 5E and 5F). In addition, the SPR data also revealed a marked binding of PND to H1N1/Cal09 and H3N2/Aichi HA proteins with the KD values of 6.9 μM and 7.3 μM, respectively (Figures 5G and 5J). The binding of H1N1/Cal09 and H3N2/Aichi HA proteins to the positive control 3′-SL and arbidol were also confirmed by SPR assay (Figures 5H, 5I, 5K, and 5L). Taken together, PND may block IAV infection through direct interaction with virus HA protein.

Identification of the potential binding sites of PND to virus HA protein

To explore the accurate binding site of PND on HA protein, the escape mutant viruses were screened through passaging an IAV for eight passages with continuous treatment of PND (25 μg/ml). The results showed that the obvious CPE occurred after the 7^{th} passage (Figure 6A), and the viral HA titers increased to more than 80% of that in virus control group post the 7^{th} passage (Figure 6B), suggesting that the escape mutant viruses may be produced at 7^{th} and 8^{th} passages. To confirm this notion, we evaluated the sensitivity of PND-selected escape mutant viruses (PR8-EM) and wild type virus

(PR8-WT) to PND using the HA assay. The wild type PR8 was still sensitive to PND with an IC_{50} value of about 6 μg/ml, while the selected virus at the 7th and 8th passages exhibited resistance to PND with IC_{50} values > 42 μg/ml (Figure 6C).

Sequence analysis revealed that the PND treated 7th passage virus had four nucleotide mutations, which produced three amino acid mutations (T30N, E233D and T359A) and one silent mutation (Q529Q) (Figure 6C). The first T30N mutation is located at the 13 position of the HA1 subunit, which is the potential site of N-glycosylation (NST) (Figure 6D). The second E233D mutation was located in the 216 position of the HA1 subunit but did not change the charge properties of the resulting amino acid. However, the third T359A mutation was in the 15 position of the HA2 subunit, which is located at the fusion peptide domain of HA2 (1-23 aa), suggesting that this site may be related to the inhibition of membrane fusion by PND (Figure 6D).

To further explore the binding modes of PND at H1 hemagglutinin, molecular docking was performed with HA protein 1RU7 (H1) using MOE software.[31] The probable binding sites on hemagglutinin were predicted using the 'binding site finding' module in MOE. The stability of the predicted conformations of the PND-HA complex was evaluated by the average root-mean-square deviation (rmsd) value of HA protein and PND. As shown in Figures 6E and 6F, after 50 ns MD the compound PND was positioned at the binding site consisting of residues mostly from the B chain of HA protein including B11E, B14W, B15T, B16G, B25H, B34Y, B135N and B137C, and only one residue, A8C, from the A chain. PND contains three aromatic rings, one indole ring in the middle with two benzene rings on its two sides. The middle indole ring was oriented to the center of the binding site forming T-pi interactions with the indole ring of B14W, and van der Waals

contacts with the side chains of B34Y, B25H, and B135N, and the disulfide bond between B137C and A8C. One of the substituted benzene rings formed van der Waals contacts with the side chain of B11E, with the other ring forming van der Waals interactions with B15T and a hydrogen bond with the backbone NH hydrogen of B16G (Figure 6F). Thus, B15T (T359) was suggested to be the main binding site of PND to virus HA protein.

Mechanism of viral entry inhibition by PND

To explore whether the inhibition of HA by PND is associated with virus endocytosis, the indirect immunofluorescence assay was peroformed by using anti-NP antibodies in IAV infected cells. The results showed that PND treatment (25 μg/ml) during an early infection stage (0-2 h p.i.) significantly reduced the green fluorescence of NP protein in both cytoplasm and nucleus as compared to the control group, suggesting that PND can block IAV endocytosis and nuclear import of viral RNP (Figure 7A).

Moreover, viral fusion with the host cell membrane is mediated by a large conformational change in cleaved HA protein (HA1+HA2) that is triggered by the low pH. To directly assess inhibition of the HA rearrangements that are associated with fusion activation by PND, we performed conformational change inhibition (CCI) assay (Figure 7B).[32] The results showed that after acidification and DTT treatment, there was only about 13% of HA1 subunit on HA proteins, however, PND treatment (50, 25 μg/ml) before acidification significantly increased the retention amount of HA1 subunit on HA proteins ($P<0.05$), suggested that PND prevents the conformational change at low pH in the CCI assay (Figure 7C).

Because the T359A (T15 in HA2) mutation site in mutant PR8 virus (Figure 6C) is close to the cleavage site of HA0, we further explored whether PND could block trypsin cleavage of HA0 into the HA1 and HA2 subunits by using a trypsin susceptibility (TS) assay. The results showed that HA was cleaved completely under both neutral and acidic conditions (Figure S19), indicating that PND was unable to provide a protective effect on HA. Thus, inhibition of the trypsin-mediated cleavage of HA0 is not the mechanism of PND.

To further explore the mechanism of viral entry inhibition by PND, we subsequently generated the PR8/H1N1 pseudoviruses (IAV-GFP) with the wild type (WT) HA protein or mutated HA proteins (T30N/E233D/T359A or T359A) to verify the interaction of PND with HA proteins. As shown in Figures 7D and 7E, PND pretreatment significantly reduced the amount of GFP positive cells comparing to the non-treated virus control group ($p < 0.01$), suggesting that PND can block the infection of IAV-GFP pseudovirus with wild type HA protein. However, PND pretreatment can hardly reduce the infection of IAV-GFP with mutated HA proteins (T30N/E233D/T359A or T359A) (Figures 7D, 7F and 7G), suggesting that both the three point mutation (T30N/E233D/T359A) and the single point mutation (T359A) can all abolish the inhibition of HA protein by PND. The result indicated that T359 site (T15 in HA2) may be indispensable for the interaction between PND and HA proteins.

Taken together, PND can primarily interact with the two threonine residues (HA2-T15 and HA1-T17) in both the HA1 and HA2 subunits to interfere with conformational change of HA protein at low pH so as to block viral entry process.

CONCLUSION

In this study, we reveal that clavatol is a chemoreactive *o*-QM equivalent and possesses a non-enzymatically multipotent behavior. Based upon this feature, we constructed 15 new clavatol-oriented pseudo natural products by mimicking the biosynthesis process of the penilactiones. In sharp contrast to penilactone A that shows no activity against influenza A virus, PND was found to exhibit potent and broad-spectrum anti-IAV activities with low risk of inducing drug resistance. The subsequent study of action mechanism by aid of HI and HA syncytium assays, escape mutant virus selection, immunofluorescence assay etc. indicated that PND can target both the HA1 and HA2 subunits of HA which are involved in virus attachment to host cells and subsequent entry via fusion of the viral membrane to the host cell membrane.[21] The results of SPR assay and CCI assay further verified that PND can truly interact with HA protein to block its conformational change.

PND, possessing a novel structure scaffold, is the first dual inhibitor of HA protein that blocks both virus entry and membrane fusion processes. Recently, targeting hemagglutinin has emerged as a promising strategy for inhibiting epidemic influenza A virus. Several small molecules targeting hemagglutinin have been identified as novel antiviral drug candidates, including HA1-binding compounds (e.g., sialic acid analogs),[33] HA2 based fusion inhibitors (e.g., arbidol, TBHQ, and JNJ4796),[34-36] and HA0 cleavage inhibitors (e.g., nafamostate).[37] Although HA1 binding agents or HA0 cleavage inhibitors may block early viral infection, concerns regarding drug resistance and side effects still remain.[38] Arbidol (Phase III pipeline) binds in a hydrophobic cavity in the HA trimer stem like another HA fusion inhibitor, TBHQ, and functions as a molecular glue to stabilize

the HA trimer, which is different from the HA-targeting antibodies and from other class I fusion protein inhibitors.[34] However, one major drawback of arbidol is that a large dose must be administered to achieve peak plasma concentration and therapeutic efficacy.[21] PND interacts with two threonine residues in both the HA1 and HA2 subunits and showed inhibition effects against many different subtypes of IAVs, superior to the effects of arbidol. More importantly, intranasal or oral administration of PND at low doses was shown to protect mice against IAV-induced death and weight loss, superior to the effects of oseltamivir, a popular anti-IAV drug. Thus, developing a drug that inhibits multiple HA functions such as receptor binding and membrane fusion will be effective for therapy of influenza diseases. Evaluation of more PND derivatives is underway to improve oral bioavailability, similar to GS4071 (4.3%) the active parent compound of the prodrug Oseltamivir.[39] Also, Our findings uncover that the use of reactive intermediates could expand our understanding of chemical diversity and aid in drug development.

EXPERIMENTAL SECTION

General experimental procedures. Specific rotations were obtained on a JASCO P-1020 digital polarimeter. UV spectra were recorded on a Beckman DU 640 spectrophotometer. IR (KBr) spectra were recorded with a Nicolet NEXUS 470 spectrophotometer. 1D and 2D NMR spectra were recorded on a JEOL JNM-ECP 600 spectrometer, or a Bruker Avance 400 using TMS as internal standard, and chemical shifts were recorded as δ values. ESIMS was obtained on a Thermo Scientific LTQ Orbitrap XL mass spectrometer or a Micromass Q-TOF ULTIMA GLOBAL GAA076 LC Mass spectrometer. Semiprepartive HPLC was performed using an ODS column [HPLC

(YMC-Pack ODS-A, 10 × 250 mm, 5 *μ*m, 4 mL/min)]. Column chromatography (CC) were performed with silica gel (300–400 mesh, Qingdao Marine Chemical Inc., Qingdao, People's Republic of China), and Sephadex LH-20 (Amersham Biosciences), respectively.

Fungus strain and supplementary experiment. Isolation and identification of the fungal strain *Penicillium crustosum* PRB-2 was described in a previous study by our group[18]. The culture conditions and fermentation medium were the same with those as previously reported. The exogenous substrates **i**-**xi** were dissolved in DMSO, then filtered by 0.22 *μ*m filter, separately before adding into culture medium. 600 mL fermentation of PRB-2 was prepared under static conditions for 30 days at room temperature and the final concentration of each substrate in medium was 150 mg/L. After 30 days of cultivation, 600 mL of whole broth was crushed and extracted with EtOAc (600 mL × 3). The EtOAc solution was concentrated under reduced pressure to give the crude extract.

UPLC-MS analysis of extract and structure purification. Analyzed by UPLC-MS, the extracts containing new peaks were selected and chromatographed on SephadexLH-20 with MeOH. Guided by the UPLC-MS data, the fractions with target compounds were further separated by MPLC (C-18 ODS) using MeOH-H_2O (a gradient elution, 5%-100%), then purified by semi-preparative HPLC (MeOH-H_2O (30%-100%), with 1/1000 formic acid in H_2O). By the method above, addition of indole (**i**), indole-3-carboxaldehyde (**ii**) or indole-3-carboxylic acid (**iii**) resulted in common generation of monoclavatol- and biclavatol-based indole alkaloids (**1** and **2**). Addition of 2-phenylindole (**iv**) led to monoclavatol adduct **3**. The peak from addition of 3,5-

di(trifluoromethyl)aniline (**ix**) could not obtained by this method and it was purified by semi-preparative HPLC with CH3CN-H2O (30%-100%) to give the monoclavatol adduct **4** successfully.

Systhesis of compound 5-15. Compound **xii** was synthesized as previously reported. Reaction of **vi**-**viii** and **x**-**xi** with **xii** in dioxane at 110 ^{o}C for 3 h yielded 11 additional clavatol-containing alkaloids (**5**-**15**).

The compounds **1**-**15** were elucidated by 1D and 2D NMR, UV absorption and HRESIMS. Before performing on NMR spectra and a series of bioactive experiments, all corresponding compounds were purified to >95% purity by HPLC and double checked by ^{1}H NMR spectra (the detailed information has shown in Supplementary information).

Compound **1**: pale yellow powder, UV (MeOH) λ_{max} (log ε): 226 (4.02), 287 (3.73), 330 (3.31); IR (KBr) ν_{max} 3450, 1683, 1648, 1540, 1456 cm^{-1}; The ^{13}C and ^{1}H NMR data, see Supplementary Table 1; HRESIMS $[M+H]^+$ 296.1280 (calcd. for $C_{18}H_{18}O_3N$, 296.1281).

Penindolone **(2)**: pale yellow powder, UV (MeOH) λ_{max} (log ε): 230 (4.06), 281 (3.77), 331 (3.31); IR (KBr) ν_{max} 3345, 1625, 1481, 1330, 1191, 1076cm^{-1}; The ^{13}C and ^{1}H NMR data, see Supplementary Table 2; HRESIMS $[M+H]^+$ 474.1910 (calcd. for $C_{28}H_{28}O_6N$, 474.1911).

Compound **3**: pale yellow powder, UV (MeOH) λ_{max} (log ε): 231 (3.92), 289 (3.64); IR (KBr) ν_{max} 3441, 3298, 1626, 1292, 1196, 1078, 744, 699 cm^{-1}; The ^{13}C and ^{1}H NMR data, see Supplementary Table 2; HRESIMS $[M+H]^+$ 372.1603 (calcd. for $C_{24}H_{22}O_3N$, 372.1594).

Compound **4**: pale yellow powder, UV (MeOH) λ_{max} (log ε): 231 (3.99), 267 (3.72), 330 (3.30); IR (KBr) ν_{max} 3398, 1672, 1277, 1201, 1133, 725 cm^{-1}; The ^{13}C and ^{1}H NMR data, Supplementary Table 3; HRESIMS $[M+H]^+$ 408.1029 (calcd. for $C_{18}H_{16}O_3NF_6$, 408.1029).

Compound **5**: pale yellow powder, UV (MeOH) λ_{max} (log ε): 229 (4.01), 283 (3.67), 334 (3.31); IR (KBr) ν_{max} 3272, 1591, 1370, 1282, 1188, 1074, 784 cm^{-1}; The ^{13}C and ^{1}H NMR data, see Supplementary Table 2; HRESIMS $[M+H]^+$ 474.1911 (calcd. for $C_{28}H_{28}O_6N$, 474.1911).

Compound **6**: pale yellow powder, UV (MeOH) λ_{max} (log ε): 231 (3.92), 286 (3.77), 328 (3.09); IR (KBr) ν_{max} 3332, 1602, 1285, 1187, 1080, 743 cm^{-1}; The ^{13}C and ^{1}H NMR data, see Supplementary Table 4; HRESIMS $[M+H]^+$ 652.2558 (calcd. for $C_{38}H_{38}O_9N$, 652.2541).

Compound **7**: pale yellow powder, UV (MeOH) λ_{max} (log ε): 239 (4.03), 287 (3.71), 340 (3.31); IR (KBr) ν_{max} 3403, 3306, 1599, 1371, 1334, 1172, 1069, 731 cm^{-1}; ^{1}H NMR (500 MHz, DMSO-d_6): δ 12.93 (s, 1H), 10.92 (s, 1H), 7.63 (s, 1H), 7.33 (d, J = 8.1 Hz, 1H), 7.16 (d, J = 7.6 Hz, 1H), 6.94 (t, J = 7.8 Hz, 1H), 6.35(s, 1H), 4.33 (s, 2H), 2.55 (s, 3H), 2.18(s, 3H); ^{13}C NMR (125 MHz, DMSO-d_6): 203.4, 161.7, 161.2, 138.5, 131.6, 125.5, 123.9, 122.7, 122.4, 116.6, 114.2, 113.8, 113.8, 112.6, 111.6, 26.7, 20.7, 16.8; HRESIMS $[M+H]^+$ 374.0387 (calcd. for $C_{18}H_{17}O_3NBr$, 374.0386).

Compound **8**: pale yellow powder, UV (MeOH) λ_{max} (log ε): 243 (3.98), 282 (3.75), 335 (3.41); IR (KBr) ν_{max} 3402, 3306, 1599, 1355, 1173, 1070, 731 cm^{-1}; ^{1}H NMR (500 MHz, DMSO-d_6): δ 12.96 (s, 1H), 12.90 (s, 1H), 10.16 (s, 1H), 7.54 (s, 1H), 7.50 (s, 1H),

7.24 (d, J = 8.1 Hz, 1H), 7.06 (d, J = 7.6 Hz, 1H), 6.77 (t, J = 7.8 Hz, 1H), 4.48 (s, 2H), 3.72 (s, 2H), 2.53 (s, 3H), 2.50 (s, 3H), 2.11 (s, 3H), 2.07 (s, 3H); ^{13}C NMR (125 MHz, DMSO-d_6): δ 203.4, 201.2, 162.0, 161.4, 161.3, 161.1, 137.5, 136.8, 136.8, 132.0, 131.1, 126.4, 123.3, 120.7, 116.6, 116.3, 115.1, 114.8, 112.8, 112.4, 111.8, 111.1, 26.6, 26.5, 20.1, 19.0, 16.9, 16.8. HRESIMS $[M+H]^+$ 552.1014 (calcd. for $C_{28}H_{27}O_6NBr$, 552.1016).

Compound **9**: pale yellow powder, UV (MeOH) λ_{max} (log ε): 239 (4.00), 287 (3.77), 332 (3.31); IR (KBr) ν_{max} 3497, 3204, 1589, 1327, 1190, 1071, 729 cm^{-1}; ^{1}H NMR (500 MHz, DMSO-d_6): δ 13.11 (s, 1H), 12.89 (s, 1H), 7.65 (s, 1H), 7.64 (d, J = 8.1 Hz, 1H), 7.64 (s, 1H), 7.61 (s, 1H), 7.15 (d, J = 7.6 Hz, 1H), 6.97 (t, J = 8.0 Hz, 1H), 6.55 (s, 1H), 5.12 (s, 2H), 4.30 (s, 2H), 2.57 (s, 3H), 2.49 (s, 3H), 2.17 (s, 3H), 2.09 (s, 3H); ^{13}C NMR (125 MHz, DMSO-d_6): δ 203.7, 203.5, 161.4, 161.4, 161.3, 161.2, 138.2, 133.5, 131.6, 128.5, 125.4, 122.7, 122.2, 116.6, 116.4, 113.8, 113.7, 113.1, 112.7, 112.5, 111.4, 110.4, 38.4, 26.7, 26.6, 20.6, 16.8, 16.7. HRESIMS $[M+H]^+$ 552.1008 (calcd. for $C_{28}H_{27}O_6NBr$, 552.1016).

Compound **10**: pale yellow powder, UV (MeOH) λ_{max} (log ε): 231 (4.02), 284 (3.69), 338 (3.34); IR (KBr) ν_{max} 3498, 3183, 1621, 1328, 1191, 1071, 968, 730 cm^{-1}; ^{1}H NMR (500 MHz, DMSO-d_6): δ 13.31 (s, 1H), 12.93 (s, 1H), 12.91 (s, 1H), 7.56 (s, 1H), 7.51 (d, J = 8.3 Hz, 1H), 7.32 (s, 1H), 7.26 (s, 1H), 7.07 (d, J = 7.6 Hz, 1H), 6.83 (d, J = 8.0 Hz, 1H), 5.34 (s, 2H), 4.36 (s, 2H), 4.24 (s, 2H), 2.47 (s, 3H), 2.46 (s, 3H), 2.38 (s, 3H), 2.08 (s, 3H), 1.96 (s, 3H), 1.89 (s, 3H); ^{13}C NMR (125 MHz, DMSO-d_6): 203.0, 203.0, 203.0, 161.4, 161.4, 161.4, 161.1, 161.1, 161.1, 137.8, 134.8, 133.1, 131.4, 130.2, 128.8, 125.6, 123.7, 121.6, 121.3, 116.8, 116.3, 113.3, 113.0, 112.1, 112.0, 111.4,

111.0, 110.3, 110.0, 37.4, 26.5, 26.5, 26.4, 20.1, 20.0, 16.8, 16.7, 16.2; HRESIMS $[M+H]^+$ 732.1626 (calcd. for $C_{38}H_{37}O_9NBr$, 732.1626).

Compound **11**: pale yellow powder, UV (MeOH) λ_{max} (log ε): 233 (4.01), 282 (3.74), 335 (3.35); IR (KBr) ν_{max} 3406, 1682, 1648, 1540, 1456, 1109 cm^{-1}; ^1H NMR (500 MHz, DMSO-d_6): δ 12.99 (s, 1H), 10.49 (s, 1H), 9.51 (s, 1H), 7.55 (s, 1H), 7.44 (s, 1H), 7.16 (d, J = 8.2 Hz, 1H), 6.83 (d, J = 8.2 Hz, 1H), 6.80 (d, J = 2.25 Hz, 1H), 3.95 (s, 2H), 2.52 (s, 3H), 2.35 (s, 3H), 2.15 (s, 3H); ^{13}C NMR (125 MHz, DMSO-d_6): δ 203.7, 161.0, 160.9, 134.8, 131.2, 127.9, 126.7, 123.3, 122.7, 118.9, 116.4, 115.4, 113.0, 112.9, 111.3, 26.7, 21.9, 18.3, 16.8; HRESIMS $[M+H]^+$ 310.1438 (calcd. for $C_{19}H_{20}O_3N$, 310.1438).

Compound **12**: pale yellow powder, UV (MeOH) λ_{max} (log ε): 230 (3.99), 287 (3.67), 340 (3.33); IR (KBr) ν_{max} 3346, 2924, 1626, 1331, 1192, 744 cm^{-1}; ^1H NMR (500 MHz, DMSO-d_6): δ 13.08 (s, 1H), 13.04 (s, 1H), 9.59 (s, 1H), 7.59 (s, 1H), 7.52 (s, 1H), 7.23 (s, 1H), 7.06 (d, J = 8.2 Hz, 1H), 6.66 (d, J = 8.3 Hz, 1H), 4.20 (s, 2H), 4.04 (s, 2H), 2.53 (s, 3H), 2.51 (s, 3H), 2.22 (s, 3H), 2.17 (s, 3H), 2.15 (s, 3H); ^{13}C NMR (125 MHz, DMSO-d_6): δ 203.5, 203.5, 161.2, 161.2, 161.2, 161.2, 135.1, 133.8, 131.7, 131.1, 128.7, 126.1, 121.3, 118.6, 116.5, 116.3, 115.5, 113.5, 112.8, 112.6, 110.8, 108.4, 26.6, 26.6, 22.0, 20.2, 18.2, 16.9, 16.9. HRESIMS $[M+H]^+$ 488.2063 (calcd. for $C_{29}H_{30}O_6N$, 488.2068).

Compound **13**: pale yellow powder, UV (MeOH) λ_{max} (log ε): 231 (3.94), 286 (3.76), 339 (3.31); IR (KBr) ν_{max} 3242, 1591, 1307, 1188, 1074, 768 cm^{-1}; ^1H NMR (500 MHz, DMSO-d_6): δ 13.17 (s, 1H), 12.99 (s, 1H), 7.64 (s, 1H), 7.53 (s, 1H), 7.47 (d, J = 8.2 Hz, 1H), 7.41 (s, 1H), 6.98 (s, 1H), 6.86 (d, J = 8.4 Hz, 1H), 5.14 (s, 2H), 3.89 (s, 2H), 2.52

(s, 3H), 2.52 (s, 3H), 2.33 (s, 3H), 2.14 (s, 3H), 2.13 (s, 3H); ^{13}C NMR (125 MHz, DMSO-d_6): δ 203.80, 203.63, 161.41, 160.94, 160.89, 160.89, 134.9, 133.4, 131.2, 128.0, 127.5, 126.6, 122.5, 119.0, 116.6, 116.3, 115.3, 112.7, 112.7, 112.1, 111.9, 110.2, 37.9, 26.7, 26.7, 21.8, 18.2, 16.8, 16.7; HRESIMS $[M+H]^+$ 488.2059 (calcd. for $C_{29}H_{30}O_6N$, 488.2068).

Compound **14**: pale yellow powder, UV (MeOH) λ_{max} (log ε): 235 (4.00), 289 (3.73), 334 (3.20); IR (KBr) ν_{max} 3471, 3332, 1592, 1285, 1188, 862, 744 cm^{-1}; ^{1}H NMR (500 MHz, DMSO-d_6): 13.08 (s, 2H), 12.99 (s, 1H), 7.54 (s, 1H), 7.50 (s, 1H), 7.47 (s, 1H), 7.13 (d, J = 8.2 Hz, 1H), 7.09 (s, 1H), 6.60 (d, J = 8.5 Hz, 1H), 5.27 (s, 2H), 4.50 (s, 2H), 3.99 (s, 2H), 2.46 (s, 6H), 2.16 (s, 3H), 2.10 (s, 3H), 2.09 (s, 3H), 2.08 (s, 3H), 2.08 (s, 3H); ^{13}C NMR (125 MHz, DMSO-d_6): δ 203.4, 203.4, 161.6, 161.3, 161.3, 161.2, 138.2, 134.6, 132.9, 131.5, 130.9, 128.2, 126.2, 121.2, 118.4, 116.5, 116.2, 115.0, 113.5, 112.5, 112.5, 112.4, 111.6, 109.7, 108.3, 36.9, 26.6, 26.6, 21.8, 19.8, 18.8, 16.8, 16.7; HRESIMS $[M+H]^+$ 666.2705 (calcd. for $C_{39}H_{40}O_9N$, 666.2698).

Compound 15: pale yellow powder, UV (MeOH) λ_{max} (log ε): 228 (4.02), 279 (3.66), 330 (3.31); IR (KBr) ν_{max} 3209, 3091, 1677, 1367, 1294, 1187, 1128, 721 cm^{-1}; The ^{13}C and ^{1}H NMR data, see Table 1 and Table 2, respectively; HRESIMS $[M+H]^+$ 286.1432 (calcd. for $C_{17}H_{20}O_3N$, 286.1438).

For other experimental details see the supplementary material.

Cells and virus. MDCK cells were grown in RPM1640 medium supplemented with 10% FBS, 100 U/mL of penicillin and 100 μg/ml of streptomycin. Influenza H1N1 virus (A/Puerto Rico/8/34; PR/8) was propagated in 10-day-old embryonated eggs for three

days at 36.5 °C. Influenza H1N1 virus (A/California/04/2009; Cal09) and H3N2 virus (A/swine/Minnesota/02719/2009; Minnesota) were propagated in MDCK cells for three days at 37 °C. For infection, virus propagation solution was diluted in PBS containing 0.2% bovine serum albumin (BSA) and was added to cells at the indicated multiplicity of infection (MOI). Virus was allowed to adsorb 60 min at 37 °C. After removing the virus inoculum, cells were maintained in infecting media (RPM1640, 4 μg/ml trypsin) at 37 °C in 5% CO_2.

Cytopathic effect (CPE) inhibition assay. The cytopathic effect (CPE) inhibition assay was performed as described previously.[22,23] MDCK cells in 96-well plates were firstly infected with IAV (MOI=0.1), and then treated with different compounds in triplicate after removal of the virus inoculum. After 48 h incubation, the cells were fixed with 4% formaldehyde for 20 min at room temperature (RT). After removal of the formaldehyde, the cells were stained with 0.1% crystal violet for 30 min. The plates were then washed and dried followed by solubilization of the dye with methanol, and the intensity of crystal violet staining for each well was measured at 570 nm.

Plaque assay. Confluent cell monolayers in 6 well plates were incubated with 10-fold serial dilutions of IAV at 37 °C for 1 h. The inoculum was removed; cells were washed with PBS and overlaid with maintenance DMEM medium containing 1.5% agarose, 0.02% DEAE-dextran, 1 mM L-glutamine, 0.1 mM non-essential amino acids, 100 U/ml penicillin, 100 μg/ml streptomycin and 1 μg/ml TPCK-treated trypsin. After incubation for 3 days at 37 °C in a humidified atmosphere of 5% CO2, cells were fixed with 0.05% glutaraldehyde, followed by staining with 1% crystal violet in 20% ethanol for plaque counting.

Hemagglutination (HA) assay. The hemagglutination (HA) assay was performed as previously reported.[27] Standardized chicken red blood cell (cRBC) solutions were prepared according to the WHO manual.[40] Virus propagation solutions were serially diluted 2-fold in round bottomed 96-well plate and 1% cRBCs were then added at an equal volume. After 60 min incubation at 4 ºC, RBCs in negative wells sedimented and formed red buttons, whereas positive wells had an opaque appearance with no sedimentation.

HA syncytium assay. The HA syncytium assay was performed as previously described with some modification.[30] In brief, Vero cells were transfected with of the PR8 HA plasmid (2 μg per well) using Lipofectamine and Plus reagent (Invitrogen). At 16 h post-transfection, the HA was first cleaved by incubation with 5 μg/mL TPCK-trypsin for 15 min at 37 °C. After pre-incubation with test compound during 15 min at 37 °C, the cells were incubated with a PH 5.0 buffer containing test compound. After exactly 10 min of incubation at 37 °C, the cells were rinsed, and medium containing 10% FBS was added, followed by 2 h of incubation at 37 °C. Finally, the cells were stained with the Hema3Stat Pak (Fisher Scientific, USA) according to the manufacturer's instructions. Syncytia were visualized and photographed using a Zeiss Axio Observer inverted microscope with an attached digital camera.

Neuraminidase Inhibition Assay. The influenza neuraminidase inhibitor detection kit (Beyotime, China) was used to measure the inhibition of NA activity. Briefly, inactivated PR8 virus supernatants was added to a 96-well plate and then mixed with different compounds (diluted in 33 mM MES buffer (pH 3.5), 4 mM CaCl2) at 37 °C for 30 min. Then MUNANA (20 μM) was added as the substrate and incubated at 37 °C for 30 min.

The reaction was stopped by the addition of stop solution (25% ethanol, 0.1 M glycine, pH 10.7). Fluorescence was measured using a SpectraMax M5 plate reader with excitation and emission wavelengths of 360 and 440 nm, respectively.

Measurement of inhibitory activity on the entry of H5N1 pseudovirus. The H5N1 pseudovirus (H5N1-Luc) was prepared using plasmids encoding the HA and NA proteins of A/Thailand/1(KAN-1)/2004. In brief, 1 μg of HA plasmid, 1 μg of NA plasmid, and 3 μg of HIV backbone plasmid (pNL4-3.luc.R-E-), which contains an Env- and Vpr-defective, luciferase-expressing HIV-1 genome per well, were co-transfected into 293FT cells in a 6-well plate (60–70% confluent) using lipofectmin 2000 (Invitrogen, USA). After incubation for 48 h, the culture supernatants were harvested and stored at -80 °C. To measure the inhibitory activities of PND, H5N1 pseudovirus H5N1-Luc infected MDCK cells were treated with PND under four different treatment conditions. The amount of infected H5N1-Luc pseudovirus was determined by luciferase assay using Pierce™ Firefly Luciferase Glow Assay Kit (Thermo Scientific, USA).

Computational modeling. Molecular docking was performed using MOE employing the AMBER10:EHT forcefield.[31] The crystal structure of HA (PDB ID:1RU7) was obtained from the Protein Data Bank (http://www.rcsb.org) for the docking studies. The binding sites were identified through Site-finder tool of MOE and mutagenesis data validation. Both the ligand and the protein were protonated at physiological pH prior to docking. The induced fit docking approach was applied for consideration of the side chain flexibility of residues at the binding site. The produced conformation with the best score was selected for the analysis. Molecular dynamics (MD) simulations were carried out on the HA in complex with compound PND using the Amber 16 package.[41] GAFF

and FF14SB force fields were employed for the ligands and the receptor, respectively.[42] Prior to the MD simulations, the complex was solvated into an octahedral box of TIP3P water molecules and neutralized by ions. The system was minimized to remove unfavorable van der Waals interactions through two steps of steepest descent minimization and conjugate gradient minimization, respectively. The cutoff of the non-bonded interactions was set to 12 Å for the energy minimization process. After minimization, MD simulation was performed as previously described.[43] For all MD simulations the time step was set to 2 fs, the particle mesh Ewald (PME) method was applied to account for long-range electrostatic interactions and the lengths of the bonds involving hydrogen atoms were fixed with the SHAKE algorithm.[44,45]

Surface plasmon resonance (SPR) assay. SPR assays were conducted on a SPR biosensor instrument GE BiacoreT200 (GE, USA). H1N1/PR8 HA proteins, H1N1/Cal09 HA proteins or H3N2/Aichi HA proteins (Sino Biological Inc., Beijing, China) were firstly immobilized onto the surface of a carboxymethylated dextran sensor chip (CM5) via amino group coupling, respectively. To assess real-time binding of PND to the HA proteins on CM5 chips, PND with different concentrations (50, 15, 12.5, 6.25, 3.125, 1.5625 μM) dissolved in DMSO, was injected over the sensor chip surface with HA immobilized within 2 min, followed by a 10-min wash with 1 × PBST buffer. The sensor chip surface was then regenerated by washing with NaOH (2 mM) for 30 s. All binding experiments were carried out at 25 °C with a constant flow rate of 2 μl/s PBS buffer. To correct for non-specific binding and bulk refractive index change, a blank channel without HA was used and run simultaneously for each experiment. Then, the BiacoreT200 SPR evaluation software was used to calculate the kinetic parameters,

and the changes in mass due to the binding response were recorded as resonance units (RU).

Serial Passage Experiments and Resistant Mutation Identification. Influenza virus (A/Puerto Rico/8/34) (MOI=0.1) was pretreated with PND (25 μg/ml) at 37 °C for 1 h before infecting MDCK cells. At the end point of each passage, the viruses that developed a significant 50% CPE were harvested and subjected to the following passages. The titer sample of harvested virus at the seventh passage was subjected to sequencing. The viral RNA was isolated from the plaque-purified viruses at 7th and 8th passage with PND using an RNAiso™ Plus Kit (Takara, Japan) according to the manufacturer's protocol. Reverse transcription (RT)-PCR was carried out with the PrimerScriptTM High Fidelity RT-PCR Kit according to the manufacturer's protocol using primer pairs: Forward: 5'-TACTGGTACCATGAAGGCAAACCT-3'; Reverse: 5'-TACTTCTAGACTAGATGCATATTC-3'. PCR products were identified by agarose gel electrophoresis and ligated into the pCDNA3.1 vector (Invitrogen, USA). The purified plasmids' DNA were sequenced by Sangon Biotech, Inc. (Shanghai, China).

Generation of IAV pseudovirus with HA mutation. The PR8/H1N1 pseudovirus (IAV-GFP) was prepared using plasmids encoding the HA and NA proteins of A/Puerto Rico/8/34. In brief, 1 μg of HA plasmid encoding wild type HA or mutated HA (T30N/E233D/T359A or T359A), 1 μg of NA plasmid, 1 μg HIV backbone plasmid (pCMV-dR8.2 dvpr), and 1 μg of reporter GFP plasmid (pLenti-CMV-GFP-Puro) were co-transfected into 293FT cells in a 6-well plate (60–70% confluent) using lipofectmin 2000 (Invitrogen, USA). After incubation for 48 h, the culture supernatants were harvested and stored at -80 °C. To measure the inhibitory activities of PND, these PR8

pseudoviruses (IAV-GFP) were pretreated with PND (50 *μ*g/ml) at 37 °C for 1 h before infection, respectively. At 48 h p.i., the amount of infected pseudovirus was observed using an inverted fluorescence microscope (DMI6000B; Leica, Germany) equipped with a cooled CCD camera.

Trypsin Susceptibility (TS) Assay. In the TS assay, ~ 5 μg PR8 HA protein was pre-incubated separately with ~ 50 μg/ml of PND for 30 min at room temperature (RT). Control reactions were incubated with 2% DMSO. The pH of each reaction was lowered using 1M sodium acetate buffer (pH 5.0). One reaction was retained at pH 7.0 to assess digestion at neutral pH. The reaction solutions were then thoroughly mixed and incubated for 20 min at 37 °C. After incubation, the reaction solutions were equilibrated at RT and the pH was neutralized by addition of 200 mM Tris buffer, pH 8.5. TPCK treated trypsin (Sigma, USA) to all samples at final ratio of 1:50 by mass and the samples were digested for 30 minutes at 37 °C. After incubation with trypsin, the reaction solutions were equilibrated at RT and quenched by addition of non-reducing SDS buffer and boiled for ~ 2 min at 100 °C. All samples were analyzed by 12% SDS-PAGE gel and Coomassie Blue Fast Staining Solution (Beyotime, Nantong, China).

Indirect immunofluorescence assay. PR8 virus was pretreated with or without PND (25 μg/ml) for 1 h at 37 ºC before infection. Then after adsorption, the inoculum was removed and the media containing PND or DMSO were added to cells. At 2 h post infection, cells were washed with PBS and fixed with 4% paraformaldehyde for 20 min. Then cells were permeabilized using 0.5% (v/v) Triton X-100 in PBS for 5 min before incubated with 2% BSA/PBS for 1 h at 37 ºC. Cells were washed and incubated with anti-NP antibody (Santcruz, USA) overnight at 4 ºC. After washing, the cells were

incubated with FITC conjugated secondary antibody (Boster, Wuhan, China) for 50 min at 37 ºC. Nuclear DNA was labeled with 4′,6′-diamidino-2-phenylindole (DAPI) (Sigma-Aldrich, Poland, USA). Finally, cells were washed and observed using Laser Scanning Confocal Microscope (Zeiss LSM 510, Jena, Germany).

Conformational Change Inhibition (CCI) Assay. The streptavidin matrix coated 96-well plates (Beaverbio, Suzhou, China) were washed with 150 µl PBS, 0.05%Tween-20, and blocked by addition of 100 µl CCI assay buffer (PBS, 1% BSA, 0.1% Tween-20) per well. After overnight blocking, the plates were washed again followed by the addition of 50 µl C-terminal biotinylated H1/PR8 HA protein (0.2 µg/ml in assay buffer) per well. Plates were incubated at room temperature (RT) for 1 hour on a plate shaker. After that, the assay plate was washed and 50 µl of 961 dilution solution (50, 25, 12.5 µg/ml) was added to the assay plate followed by another 1 hour incubation on a plate shaker. Then 10 µl of 1 M acetate (pH 5.25) was added to all wells followed by 20 minutes on a plate shaker. The plates were washed followed by addition of 2.5 mM DTT (diluted in PBS) to reduce any postfusion HA and remove HA1. To detect the presence or absence of HA1, after 60-min incubation on a shaking platform, plates were washed and sequentially incubated with anti-HA1 head antibody (Biodragon, Beijing, China) and HRP labeled secondary antibody (in assay buffer) at RT for 1 h. The plates were then washed and 50 µl of TMB solution (Beyotime, China; ELISA Substrate) was added to the wells followed by read out for absorbance at 450 nm on a microplate reader 5 minutes later.

***In vivo* experiments.** Four-week-old female Kunming mice (average weight, 14.0 ± 2.0 g) were purchased from Beijing Vital River Laboratory Animal Technology Co., Ltd. (Beijing, China) and raised in a pathogen-free environment (23 ± 2 ºC and 55 ± 5%

humidity). All animal care and experimental procedures were performed in accordance with the National Institutes of Health Guide for the Care and Use of Laboratory Animals and approved by the Institutional Animal Care and Use Committee at Ocean University of China. Mice were inoculated intranasal with PR8 (500 PFU/mouse) diluted in 40 μL of 1 × PBS, and randomly divided into experimental groups. Two hours after inoculation, mice received oral or intranasal therapy of compound PND or placebo, and the treatments were repeated once daily for the entire experiment. Oral administration of Oseltamivir (10 mg/kg/day) was used as the positive control as described previously.[46] To be consistence, the oral dosage of PND was set to 5 and 10 mg/kg/day. Mice were weighed and euthanized on Day 4 after inoculation by spinal dislocation method, and lungs were removed and weighed. The lung specimens were homogenized in 1×PBS for determination of viral titers by plaque assay.[26] Histopathological analysis was performed using H&E staining on samples collected on Day 4 as described previously.[47]

In the survival experiments, 10 mice per group were intranasally infected with PR/8 virus (1000 PFU/mouse) at Day 0. The drug administration was repeated once daily for seven days. Mice were monitored daily for weight loss and clinical signs. If a mouse lost body weight over 25% of its pre-infection weight, it was defined as dead and humanely euthanized immediately; the rest of the mice were sacrificed at the end of experiment on 14 dpi.

Pharmacokinetic studies were performed in Kunming mice (male, 20-25 g) and in Sprague Dawley rats (male, 180-220 g). The animals were maintained under a 12 hours light/12 hours dark cycle with free access to water and chow diet, and fasted for 12 h with water ad libitum before dosing. The dosing solutions were prepared by suspending

PND in 0.5% sodium carboxymethyl cellulose for oral administration and in PEG400 for intravenous administration. The dose of PND was set to be 5 mg/kg in mice and 3.5 mg/kg in rats via gavage, while 0.5 mg/kg in mice and 0.35 mg/kg in rats intravenously via tail vein. Blood samples were taken from mice by saphenous vein bleeding and from rats by jugular vascular catheterizations before dosing and at 5, 15 and 30 min and 1, 2, 3, 4, 6, 8, 12 and 24 h after oral dose and 2, 5, 15 and 30 min and 1, 2, 4, 6, 8, 12 and 24 h after intravenous injection. Besides, mice and rats were kept in the metabolic cages (Tecniplast S.p.A., Italy) with free access to water and food 2 hours post dose. Urine and feces samples were collected before dosing and at various time points after dosing of PND. Plasma was separated by centrifuging the blood samples at 1660× g for 5 min. Feces samples were dried and grinded into powder, then homogenized with water (1:9, w/v). Plasma, urine and fecal homogenate samples were mixed with acetonitrile (nine volumes for mice plasma and two volumes for others) and N-CH3 PND (internal standard, IS, final concentration 200 ng/mL), then vortexed and centrifuged at 18880×g for 5 min twice to precipitate protein. Then the supernatant was then injected into the LC-MS/MS system for analysis.

In order to check for the toxicity associated with the treatment, Kunming mice (male, 20-25 g) were treated orally with PND (5 or 10 mg/kg/day) suspended in 0.5% sodium carboxymethyl cellulose once a day for 7 consecutive days. Mice from the control group were treated with the vehicle under similar conditions. The animals were anesthetized with isoflurane at 24 h after the last administration and serum samples were collected. Serum AST, ALT, CR, BUN, LDH, CK, CK-MB levels were determined with commercial kits (Nanjing Jiancheng Bioengineering Institute, China).

***In vitro* incubation assays.** Mice liver microsomes (MLMs), rats liver microsomes (RLMs) and human liver microsomes (HLMs) with final protein concentration 0.5 mg/mL were preincubated with NADPH-regenerating system (containing 0.011 mol/L β-nicotinamide adenine dinucleotide phosphate, 0.110 mol/L glucose 6-phosphate and 10 U/mL glucose-6-phosphate dehydrogenase) in 50 mmol/L Tris-HCl buffer (pH 7.4) at 37 °C for 5 min. Then PND were added at the final concentration of 2 μmol/L to initiate the reaction. Concomitantly, NADPH-free incubations were performed as control. All samples were placed in 37 °C for incubation, and were quenched with two volumes of acetonitrile with IS (final concentration 200 ng/mL) at 60 min, then vortex-mixed and centrifuged at 18880×g for 10 min. The supernatant was subjected to LC-MS/MS analysis. The results were expressed as the percentage of the concentration at 0 min.

LC-MS/MS analysis to detect PND. LC-MS/MS instrument (Thermo Fisher Scientific, Waltham, MA, USA) consisted of a DIODEX UltiMate 3000 UHPLC system and TSQ Quantiva triple quadrupole mass spectrometer with Xcalibur 2.2 software for data acquisition and processing. PND and IS were chromatographed by injection of a 5 μL sample into an Eclipse Plus C18 column (3.5 μm, 2.1 × 50 mm, Agilent, Santa Clara, CA, USA) at 25 °C. The mobile phase consisted of solvent A (0.1% formic acid in water) and solvent B (0.1% formic acid in acetonitrile). Separation was performed at a flow rate of 0.2 mL/min with the following gradient elution: 0.0–1.5 min, 50% solvent B; 1.5–3.5 min, a linear gradient runs from 50% to 100% solvent B; 3.5–6.0 min 50% solvent B for re-equilibration. A H-ESI source was used in the negative ion mode. The optimized ion spray voltage, ion transfer tube temperature and vaporizer temperature were set at 3500 V, 325 °C and 275 °C, respectively. The sheath gas and aux gas were nitrogen

delivered at 35 arb and 10 arb, respectively. The collision gas (argon) pressure was 2.0 mTorr. Quantification was performed using the selective reaction monitoring (SRM) transition m/z 472.3→306.2 (collision energy: 18.9 V, RF lens: 100.2) for PND and m/z 486.3→308.2 (collision energy: 26.9 V, RF lens: 119.0) for IS.

Statistical analysis. All data are representative of at least three independent experiments. Data are presented as mean ± S.D. Statistical significance was analysed using GraphPad Prism 7 software using oneway ANOVA with Turkey's test. P values < 0.05 were considered significant. Pharmacokinetic parameter estimates were carried out using non–compartmental analysis via WinNonlin Software (version 6.3, Pharsight Corporation, Mountain View, CA, USA).

ASSOCIATED CONTENT

Supporting Information

Additional figures and tables, experimental materials and methods, HPLC spectra, NMR spectra and other data related to characterization of all compounds presented in current manuscript are included in the supporting information. Molecular formula strings and some data (CSV) were also included.

AUTHOR INFORMATION

Corresponding Authors

*E-mail: D.L. (email: dehaili@ouc.edu.cn; Tel: +86 532 82031619) or to W.W. (email: wwwakin@ouc.edu.cn; Tel: +86 532 82031980).

Author Contributions

G.W., D.L. and W.W. conceived the project and wrote the paper. G.Y., Y.Y., Z.D. performed the experiments of chemistry and cell-based assays. S.Y. performed the pharmacokinetic profiling. Y.L., R.Y. performed chemical synthesis and molecular docking part, respectively. G.W., D.L., W.W., S.Y., J.L., T.Z., Q.G. discussed the results and were involved in preparation of the manuscript.

#G.W., G.Y., Y.Y. and S.Y. contributed equally.

Notes

The authors declare no competingfinancial interest.

ACKNOWLEDGMENTS

This work was supported by National Natural Science Foundation of China (81973234, 81874320), the Fundamental Research Funds for the Central Universities (201941001, 201822019), the Marine S&T Fund of Shandong Province for Pilot National Laboratory for Marine Science and Technology (Qingdao) (2018SDKJ0401-2) and Taishan Scholar Youth Expert Program in Shandong Province (tsqn201812021), NSFC-Shandong Joint Fund (U1606403), Shandong Provincial Natural Science Foundation (ZR2017MH013) and from Qingdao City (2017-CXZX01-3-6). We thank Dr. David Steinhauer from Emory University School of Medicine for providing influenza virus A/California/04/2009 and A/Minnesota/02719/2009; Dr. Zongqiang Cui from Wuhan Institute of Virology, Chinese Academy of Sciences for providing influenza virus A/Puerto Rico/8/34. We are also thankful to Jaclyn M. Winter (Department of Medicinal Chemistry, University of Utah)

and Robert Keyzers (School of Chemical and Physical Sciences, Victoria University of Wellington) for reviewing and providing valuable suggestions in the preparation of the manuscript.

ABBREVIATIONS USED

IAV, influenza A virus; PND, penindolone; o-QM, ortho-Quinone methide; HA, hemagglutination; NA, neuraminidase; CPE, cytopathic effect; HI, hemagglutination inhibition; CCI, conformational change inhibition; SPR, surface plasmon resonance; TS, trypsin Susceptibility; MOI, multiplicity of infection; RT, room temperature; RBC, red blood cell; MD, molecular dynamics; SRM, selective reaction monitoring; NMR, nuclear magnetic resonance; HRMS, high resolution mass spectrometry; SAR, structure-activity relationship; po, per os; iv, intravenous; C_{max}, maximum concentration; t_{max}, time point for maximum concentration; AUC, area under the concentration curve; MLMs, mice liver microsomes; RLMs, rats liver microsomes; HLMs, human liver microsomes; NADPH, nicotinamide adenine dinucleotide phosphate; CYP, cytochrome P450 proteins; AST, aspartate aminotransferase; ALT, alanine aminotransferase; CR, creatinine; BUN, blood urea nitrogen; LDH, lactate dehydrogenase; CK,creatine kinase; CK-MB, creatine kinase MB isoenzyme.

REFERENCES

(1) World Health Organization, Ask the Expert: Influenza Q&A, **2018**.

(2) Neumann, G.; Noda, T.; Kawaoka, Y. swine-origin H1N1 influenza virus. *Nature* **2009**, *459*, 931–939.

(3) Shen, Z.; Lou, K.; Wang, W. New Small-Molecule Drug Design Strategies for Fighting Resistant Influenza A. *Acta Pharmaceutica Sinica B* **2015**, *5* (5), 419–430.

(4) De Clercq, E. Antiviral Agents Active against Influenza A Viruses.*Nat. Rev. Drug Discov.* **2006**, *5* (12), 1015–1025.

(5) Hayden, F. G.; Pavia, A. T. Antiviral Management of Seasonal and Pandemic Influenza.*J. Infect. Dis.* **2006**, *194*, S119–S126.

(6) Lackenby, A.; Hungnes, O.; Dudman, S. G.; Meijer, A.; Paget, W. J.; A. J. Hay, A. J.; Zambon, M. C. Emergence of Resistance to Oseltamivir among Influenza A(H1N1) Viruses in Europe. *Euro. Surveillance* **2008**, *13,* 1-2.

(7) Newman, D. J.; Cragg, G. M. Natural Products as Sources of New Drugs from 1981 to 2014.*J. Nat. Prod.* **2016**, *79*, 629–661.

(8) Rix, U.; Zheng, J.; Rix, L. L. R.; Greenwell, L.; Yang, K.; Rohr, J. The Dynamic Structure of Jadomycin B and the Amino Acid Incorporation Step of Its Biosynthesis.*J. Am. Chem. Soc.* **2004**, *126*, 4496–4497.

(9) Du, L.; You, J.; Nicholas, K. M.; Cichewicz, R. H. Chemoreactive Natural Products That Afford Resistance Against Disparate Antibiotics and Toxins. *Angew. Chem. Int. Ed.* **2016**, *55*, 4220–4225.

(10) Trottmann, F.; Franke, J.; Ishida, K.; García-Altares,M.; Hertweck, C. Cyclopropanol Warhead in Malleicyprol Confers Virulence of Human- and Animal-Pathogenic Burkholderia Species. *Angew. Chem. Int. Ed.* **2019**, *58*, 14129 –14133.

(11) Hu, Y.; Potts, M. B.; Colosimo, D.; Herrera-Herrera, M. L.; Legako, A. G.; Yousufuddin, M.; White, M. A.; MacMillan, J. B. Discoipyrroles A-D: Isolation, Structure Determination, and Synthesis of Potent Migration Inhibitors from Bacillus Hunanensis.*J. Am. Chem. Soc.* **2013**, *135*, 13387–13392.

(12) Pathak, T. P.; Sigman, M. S. Applications of Ortho-Quinone Methide Intermediates in Catalysis and Asymmetric Synthesis. *J. Org. Chem.* **2011**, *76*, 9210–9215.

(13) Spence, J. T. J.; George, J. H. Biomimetic Total Synthesis of Ent-Penilactone A and Penilactone B. *Org. Lett.* **2013**, *15*, 3891–3893.

(14) Spence, J. T. J.; George, J. H. Total Synthesis of Peniphenones A-D via Biomimetic Reactions of a Common o-Quinone Methide Intermediate. *Org. Lett.* **2015**, *17*, 5970–5973.

(15) Singh, M. S.; Nagaraju, A.; Anand, N.; Chowdhury, S. *ortho*-Quinone methide (*o*-QM): a highly reactive, ephemeral and versatile intermediate in organic synthesis *RSC Adv.* **2014**, *4*, 55924–55959.

(16) Shi, W.; Dan, W. J.; Tang, J. J.; Zhang, Y.; Nandinsuren, T.; Zhang, A. L.; Gao, J. M. Natural Products as Sources of New Fungicides (III): Antifungal Activity of 2,4-Dihydroxy-5-Methylacetophenone Derivatives. *Bioorganic Med. Chem. Lett.* **2016**, *26*, 2156–2158.

(17) Yang, G.; Nenkep, V. N.; Siwe, X. N.; Leutou, A. S.; Feng, Z.; Zhang, D.; Choi, H. D.; Kang, J. S.; Son, B. W. An Acetophenone Derivative, Clavatol, and a Benzodiazepine Alkaloid, Circumdatin A, from the Marine-Derived Fungus Cladosporium. *Nat. Prod. Sci.* **2009**, *15*, 130–133.

(18) Wu, G.; Ma, H.; Zhu, T.; Li, J.; Gu, Q.; Li, D. Penilactones A and B, Two Novel Polyketides from Antarctic Deep-Sea Derived Fungus Penicillium Crustosum PRB-2. *Tetrahedron* **2012**, *68*, 9745–9749.

(19) Li, D; Yu, G.; Zhu, T.; Gu, Q.; Che, Q.;Wang, W. Process for preparation of indole alkaloid compound. PCT Int. Appl. WO2017107897, **2017**.

(20) Li, D.; Yu, G.; Zhu, T.; Gu, Q.; Che, Q.; Wang, W. Process for preparation of indole alkaloid compound. Faming Zhuanli Shenqing CN106892854, **2017**.

(21) Fan, J.; Liao, G.; Kindinger, F.; Ludwig-Radtke, L.; Yin, W. B.; Li, S. M. Peniphenone and Penilactone Formation in Penicillium Crustosum via 1,4-Michael Additions of Ortho-Quinone Methide from Hydroxyclavatol to γ-Butyrolactones from Crustosic Acid. *J. Am. Chem. Soc.* **2019**, *141*, 4225–4229.

(22) Leibbrandt, A.; Meier, C.; König-Schuster, M.; Weinmüllner, R.; Kalthoff, D.; Pflugfelder, B.; Graf, P.; Frank-Gehrke, B.; Beer, M.; Fazekas, T.; Unger, H.; Prieschl-Grassauer, E.; Grassauer, A. Iota-Carrageenan Is a Potent Inhibitor of Influenza a Virus Infection. *PLoS One* **2010**, *5*, 1–11.

(23) Wang, W.; Zhang, P.; Hao, C.; Zhang, X. E.; Cui, Z. Q.; Guan, H. S. In Vitro Inhibitory Effect of Carrageenan Oligosaccharide on Influenza A H1N1 Virus. *Antiviral Res.* **2011**, *92*, 237–246.

(24) Sriwilaijaroen, N.; Suzuki, K.; Takashita, E.; Hiramatsu, H.; Kanie, O.; Suzuki, Y. 6SLN-Lipo PGA Specifically Catches (Coats) Human Influenza Virus and Synergizes Neuraminidase-Targeting Drugs for Human Influenza Therapeutic Potential. *J. Antimicrob. Chemother.* **2015**, *70*, 2797–2809.

(25) Wang, W.; Zhang, P.; Yu, G. L.; Li, C. X.; Hao, C.; Qi, X.; Zhang, L. J.; Guan, H. S. Preparation and Anti-Influenza A Virus Activity of κ-Carrageenan Oligosaccharide and Its Sulphated Derivatives. *Food Chem.* **2012**, *133*, 880–888.

(26) Hussain, S.; Miller, J. L.; Harvey, D. J.; Gu, Y.; Rosenthal, P. B.; Zitzmann, N.; McCauley, J. W. Strain-Specific Antiviral Activity of Iminosugars against Human Influenza A Viruses. *J. Antimicrob. Chemother.* **2015**, *70*, 136–152.

(27) Chen, X.; Si, L.; Liu, D.; Proksch, P.; Zhang, L.; Zhou, D.; Lin, W. Neoechinulin B and Its Analogues as Potential Entry Inhibitors of Influenza Viruses, Targeting Viral Hemagglutinin. *Eur. J. Med. Chem.* **2015**, *93*, 182–195.

(28) Hashem, A. M.; Flaman, A. S.; Farnsworth, A.; Brown, E. G.; van Domselaar, G.; He, R.; Li, X. Aurintricarboxylic Acid Is a Potent Inhibitor of Influenza A and B Virus Neuraminidases. *PLoS One* **2009**, *4*, 14–16.

(29) Vanderlinden, E.; Vanstreels, E.; Boons, E.; ter Veer, W.; Huckriede, A.; Daelemans, D.; Van Lommel, A.; Roth, E.; Sztaricskai, F.; Herczegh, P.; Naesens, L. Intracytoplasmic

Trapping of Influenza Virus by a Lipophilic Derivative of Aglycoristocetin. *J. Virol.* **2012**, *86*, 9416–9431.

(30) Byrd-Leotis, L.; Galloway, S. E.; Agbogu, E.; Steinhauer, D. A. Influenza Hemagglutinin (HA) Stem Region Mutations That Stabilize or Destabilize the Structure of Multiple HA Subtypes. *J. Virol.* **2015**, *89*, 4504–4516.

(31) Santiago Vilar, Giorgio Cozza, S. M. Medicinal Chemistry and the Molecular Operating Environment (MOE): Application of QSAR and Molecular Docking to Drug Discovery. *Curr. Top. Med. Chem.* **2008**, *8*, 1555–1572.

(32) Kadam, R. U.; Juraszek, J.; Brandenburg, B.; Buyck, C.; Schepens, W. B. G.; Kesteleyn, B.; Stoops, B.; Vreeken, R. J.; Vermond, J.; Goutier, W.; Tang, C.; Vogels, R.; Friesen, R.H.E.; Goudsmit, J.; van Dongen, M.J.P.; Wilson, I.A. Potent Peptidic Fusion Inhibitors of Influenza Virus. *Science*, **2017**, *358*, 496–502.

(33) Sun, X.-L. Recent Anti-Influenza Strategies in Multivalent Sialyloligosaccharides and Sialylmimetics Approaches. *Curr. Med. Chem.* **2007**, *14*, 2304–2313.

(34) Kadam, R. U.; Wilson, I. A. Structural Basis of Influenza Virus Fusion Inhibition by the Antiviral Drug Arbidol. *Proc. Natl. Acad. Sci.* **2017**, *114*, 206–214.

(35) Russell, R. J.; Kerry, P. S.; Stevens, D. J.; Steinhauer, D. A.; Martin, S. R.; Gamblin, S. J.; Skehel, J. J. Structure of Influenza Hemagglutinin in Complex with an Inhibitor of Membrane Fusion. *Proc. Natl. Acad. Sci.* **2008**, *105*, 17736–17741.

(36) Van Dongen, M. J. P.; Kadam, R. U.; Juraszek, J.; Lawson, E.; Brandenburg, B.; Schmitz, F.; Schepens, W. B. G.; Stoops, B.; Van Diepen, H. A.; Jongeneelen, M.; Tang, C.; Vermond, J.; van Eijgen-Obregoso Real A.; Blokland, S.; Garg, D.; Yu, W.L.; Goutier, W.; Lanckacker, E.; Klap, J.M.; Peeters, D.C.G.; Wu, J.; Buyck, C.; Jonckers, T.H.M.; Roymans, D.; Roevens, P.; Vogels, R.; Koudstaal, W.; Friesen, R.H.E.; Raboisson, P.; Dhanak, D.; Goudsmit, J.; Wilson, I.A. A Small-Molecule Fusion Inhibitor of Influenza Virus Is Orally Active in Mice. *Science.* **2019**, *363*, eaar6221.

(37) Hosoya, M.; Matsuyama, S.; Baba, M.; Suzuki, H.; Shigeta, S. Effects of Protease Inhibitors on Replication of Various Myxoviruses. *Antimicrob. Agents Chemother.* **1992**, *36*, 1432–1436.

(38) Stamou, S. C.; Reames, M. K.; Skipper, E.; Stiegel, R. M.; Nussbaum, M.; Geller, R.; Robicsek, F.; Lobdell, K. W. Aprotinin in Cardiac Surgery Patients: Is the Risk Worth the Benefit? *Eur. J. Cardio-thoracic Surg.* **2009**, *36*, 869–875.

(39) Li, W.; Escarpe, P. A.; Eisenberg, E. J.; Cundy, K. C.; Sweet, C.; Jakeman, K. J.; Merson, J.; Lew, W.; Williams, M.; Zhang, L.; Kim, C. U.; Bischofberger, N.; Chen, M. S.; Mendel, D. B. Identification of GS 4104 as an Orally Bioavailable Prodrug of the Influenza Virus Neuraminidase Inhibitor GS 4071. *Antimicrob. Agents Chemother.* **1998**, *42*, 647–653.

(40) WHO Manual on Animal Influenza Diagnosis and Surveillance World Health Organization Department of Communicable Disease Surveillance and Response. 2002.

(41) Case, D. A.; Betz, R. M.; Cerutti, D. S.; Cheatham III, T. E.; Darden, T. A.; Duke, R. E.; Giese, T. J.; Gohlke, H.; Goetz, A. W.; Homeyer, N.; Izadi, S.; Janowski, P.; Kaus, J.; Kovalenko, A.; Lee, T. S.; LeGrand, S.; Li, P.; Lin, C.; Luchko, T.; Luo, R.; Madej, B.; Mermelstein, D.; Merz, K. M.; Monard, G.; Nguyen, H.; Nguyen, H. T.; Omelyan, I.; Onufriev, A.; Roe, D. R.; Roitberg, A.; Sagui, C.; Simmeling, C. L.; Botello-Smith, W. M.; Swails, J.; Walker, R. C.; Wang, J.; Wolf, R. M.; Wu, X.; Xiao, L.; Kollman, P. A. (2016) AMBER 2016. University of California, San Francisco.

(42) Li, M.; Wu, G..; Kaas, Q.; Jiang, T.; Yu, R. Development of Efficient Docking Strategies and Structure-Activity Relationship Study of the c-Met Type II Inhibitors. *J. Mol. Graph. Model.* **2017**, 75, 241–249.

(43) Maier, J. A.; Martinez, C.; Kasavajhala, K.; Wickstrom, L.; Hauser, K. E.; Simmerling, C. ff14SB: Improving the Accuracy of Protein Side Chain and Backbone Parameters From ff99SB. *J. Chem. Theory Comput.* **2015**, 11, 3696–3713.

(44) Miyamoto, S.; Kollman, P.; Peter, A.; Kiyamoto, S. SETTLE - An Analytical Version of the SHAKE and RATTLE Algorithm for rigid Water Models. *J. Comput. Chem.* **1992**, 13: 952–962.

(45) Darden, T.; York, D.; Pedersen, L. Particle mesh Ewald: An N-log(N) method for Ewald sums in large systems. *J. Chem. Phys.* **1993**, 98, 10089–10092.

(46) Smee, D. F.; Wong, M. H.; Bailey, K. W.; Sidwell, R. W. Activities of Oseltamivir and Ribavirin Used Alone and in Combination Against Infections in Mice With Recent Isolates of Influenza A (H1N1) and B Viruses. *Antivir. Chem. Chemother.* **2006**, 17, 185–192.

(47) Fukushi, M.; Ito, T.; Kitazawa, T.; Miyoshi-Akiyama, T.; Kirikae, T.; Yamashita, M.; Kudo, K. Serial histopathological examination of the lungs of mice infected with influenza A virus PR8 strain. *PLoS One,* **2011**, 6(6):e21207.

TABLES

Table 1. Pharmacokinetic data of PND.

Parameter	Species		
	Mouse	Rat	Human
C_{max} po (ng/mL)	16.0	286.8	ND
t_{max} po (hours)	4.0	4.3	ND
$t_{1/2}$ po / iv (hours)	- / 3.4	3.3 / 4.8	ND
$AUC_{(0\text{-}t)}$ po / iv (hours*ng/mL)	152.3 / 269.0	1362.3 / 10052.9	ND
Bioavailability po (%)	5.7	1.4	ND
Cumulative excretion in urine po / iv (% given dose after 72 hours)	0.03 / 0.3	0.004 / 0.006	ND
Cumulative excretion in feces po / iv (% given dose after 72 hours)	38.4 / 29.1	96.4 / 7.2	ND
Metabolic stability in liver microsomes (% remaining compound after 60 min)	0.8	36.6	71.6

po, per os; iv, intravenous; C_{max}, maximum concentration; t_{max}, time point for maximum concentration; AUC, area under the concentration curve; $t_{1/2}$, half-life, it was estimated on the basis of the values within 24 hours in this case so that it was missing for the samples from mice given drug orally; ND, not determined. Pharmacokinetic parameters (C_{max}, t_{max}, $t_{1/2}$, and AUC) were determined after a single oral administration of PND at 5 mg/kg in mice and 3.5 mg/kg in rats (n=3). For oral bioavailability, a single oral dose was compared to a single intravenous dose of 0.5 mg/kg in mice and 0.35 mg/kg in rats. F = [AUCoral]/[AUCiv], the ratio of exposure of an equivalent dose after nonintravenous (in this case, oral) and intravenous administration as a measure of bioavailability. The final concentration for liver microsomes incubation *in vitro* was 2 μM (n=3).

FIGURES

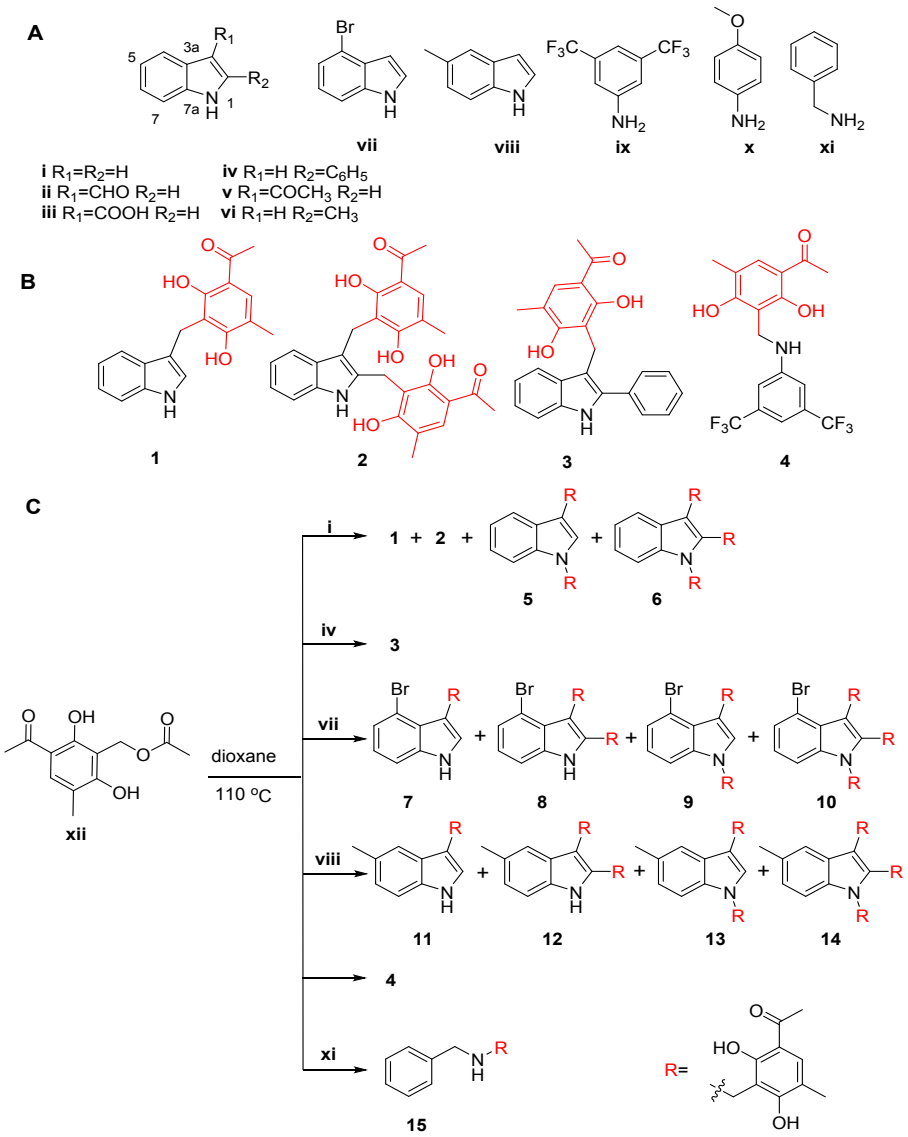

Figure 1. Structures of substrates, clavatol-based pseudo natural products, and their chemical synthesis. (A) Exogenous substrates, including indole family and aniline analogues. (B) Structures of clavatol-based pseudo natural products **1**-**4** with the clavatol moiety highlighted in red. (C) Chemical synthesis of **1**, **2** and **5**-**15**.

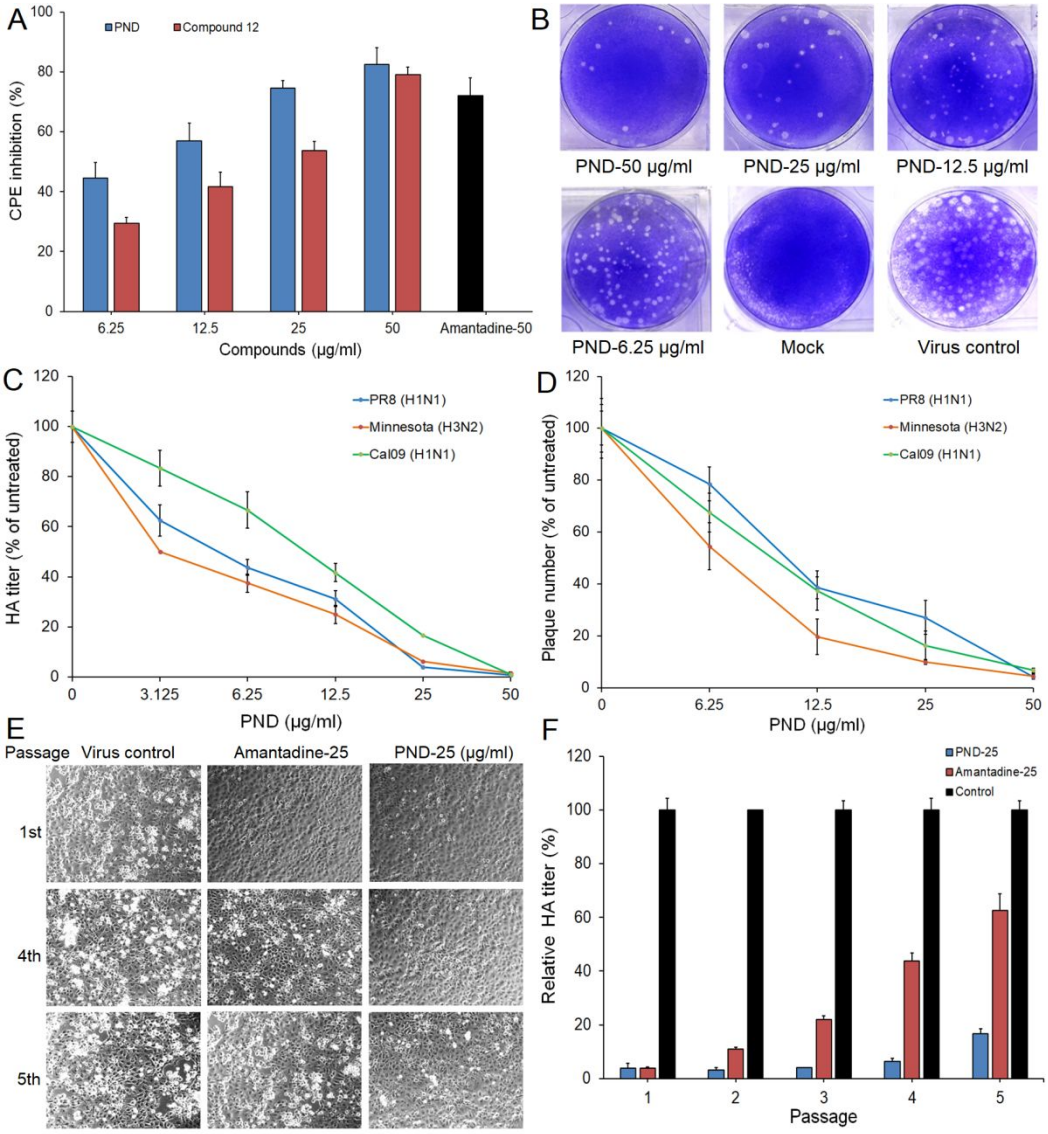

Figure 2. Compound PND (2) possesses the broad anti-IAV spectrum and low tendency of induction of viral resistance. (A)The anti-IAV (PR8; MOI = 0.1) activity was determined by CPE inhibition assay at 24 h p.i. Values are means ± S.D. (n = 5). (B) Approximately 50–100 PFU/well of PR8 virus was pre-incubated with PND(0, 6.25, 12.5, 25, 50 μg/ml) for 1 h at 37 °C before subjected to plaque reduction assay. (C and D) HA titers from single-cycle high-moi (MOI = 3.0) assays (C) and plaque numbers from plaque reduction assays (D) performed on MDCK cells infected with PR8, Minnesota and Cal09. Mean percentage HA titers and plaque numbers were calculated as a

percentage of values from untreated cells for each group. Values are means ± S.D. (n = 4). (E and F) Microscopy observations (E) of CPE at the 1st, 4th and 5th passage of a multi-passaging experiment treated by either PND or amantadine, and Quantitative analysis of the relative yield of progeny virus by HA assay at each round of total five rounds of propagation (F).

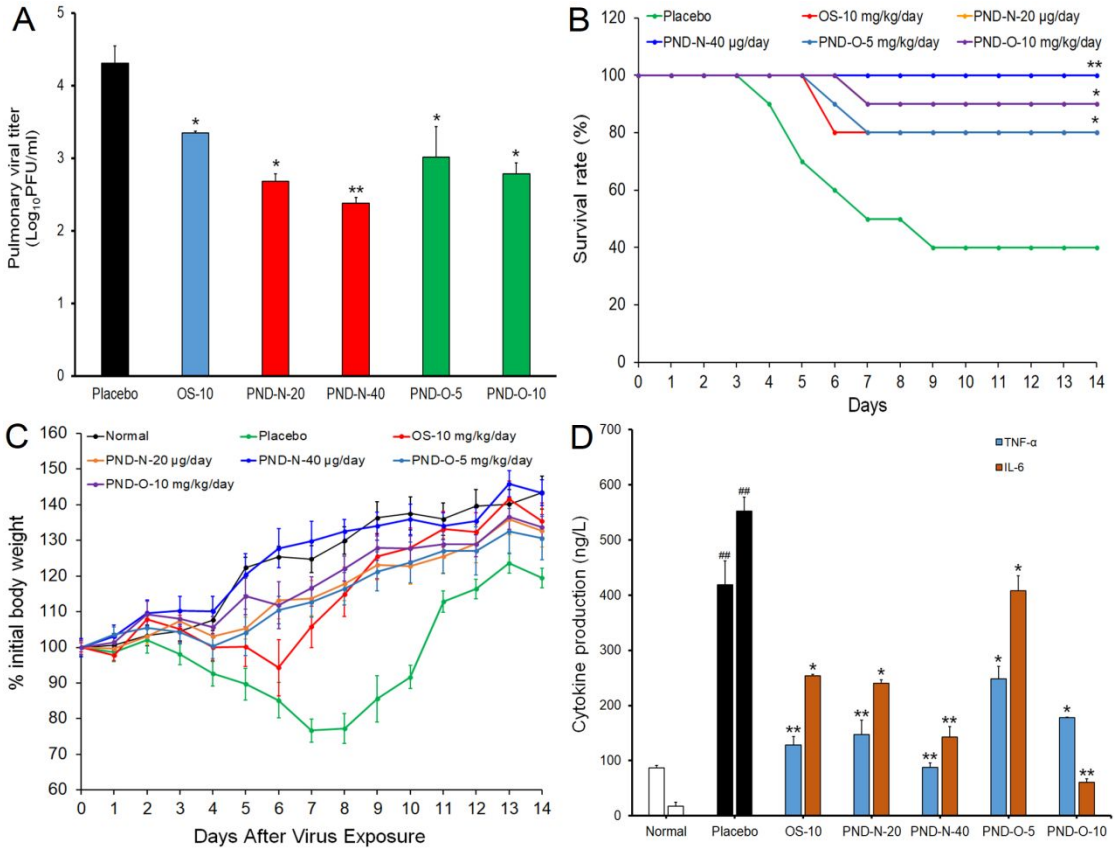

Figure 3. The anti-IAV effects of compound PND *in vivo*. (A) Viral titers in lungs. After intranasal (PND-N) or oral (PND-O) treatment with PND or oral treatment with Oseltamivir (OS) for 4 days, the pulmonary viral titers were evaluated by plaque assay. Values are means ± S.D. (n = 4). Significance: *P < 0.05, **P < 0.01 vs. virus control group. (B) Survival rate. IAV infected mice were received oral or intranasal therapy with PND for 7 days. Results are expressed as percentage of survival, evaluated daily for 14 days. (C) IAV infected mice were received oral or intranasal therapy with PND for 7 days. The body weights of six mice in each group were monitored daily for 14 days and are expressed as a percentage of the initial value. Values are means ± S.D. (n = 6). (D) After oral or intranasal therapy with PND for 4 days, the production of TNF-α and IL-6 in lung tissues was determined by ELISA assay. Values are means ± S.D. (n = 3). Significance: ##P < 0.01 vs. normal control group; *P < 0.05, **P < 0.01 vs. virus control group.

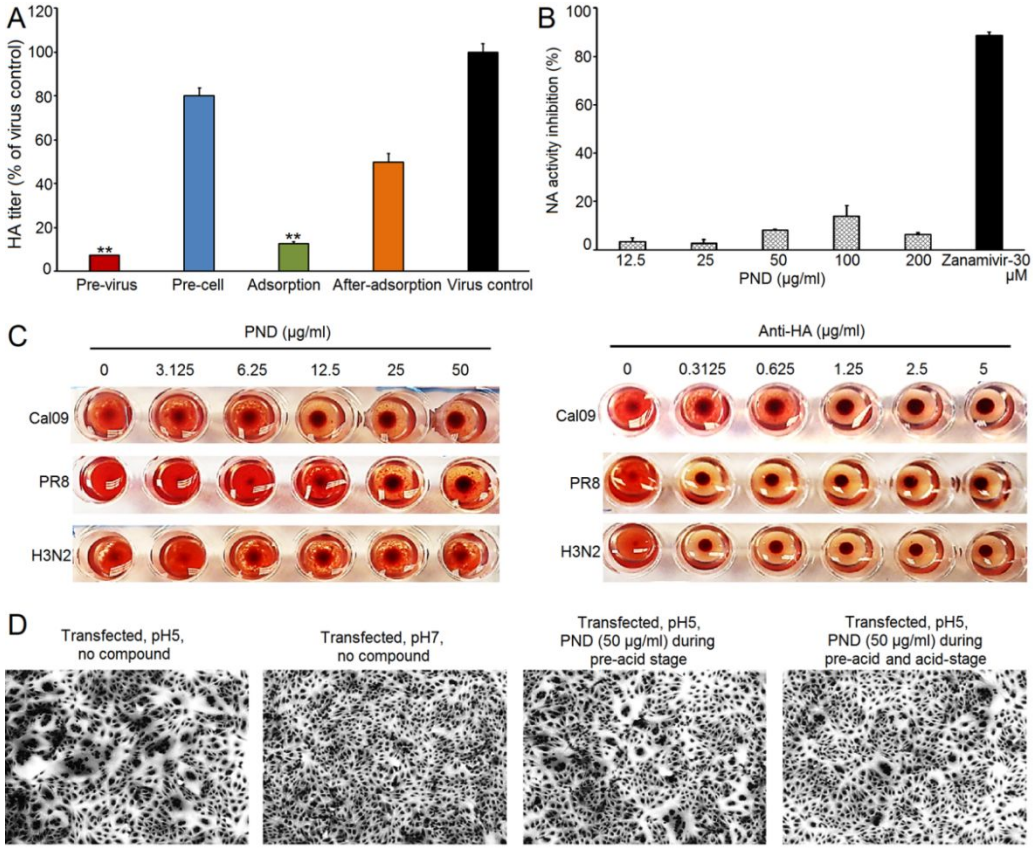

Figure 4. Compound PND may block IAV infection through direct interaction with HA protein. (A) PR8 (MOI = 1.0) infected MDCK cells were treated with PND (50 μg/ml) under four different conditions: pretreatment of virus, pretreatment of cells, during adsorption, and after adsorption. At 24 h p.i., the virus yields were determined by HA assay. Values are means ± S.D. (n = 3). Significance: *P < 0.05, **P < 0.01 vs. virus control group. (B) Inactivated PR8 virus was incubated with PND or zanamivir (30 μM), and the NA enzymatic activity was determined by a fluorescent assay. Values are means ± S.D. (n = 4). (C) The inhibition of PND and anti-HA antibody on influenza virus induced aggregation of chicken erythrocytes were evaluated by hemagglutination inhibition (HI) assay. (D) Vero cells expressing PR8 HA were firstly treated with trypsin, and then incubated with or without PND (50 μg/ml). Then, the pH was lowered to 5.0 and the cells were incubated with PND. Following syncytium formation for 2 h at 37°C, the cells were stained with Hema3Stat Pak, and examined by microscopy.

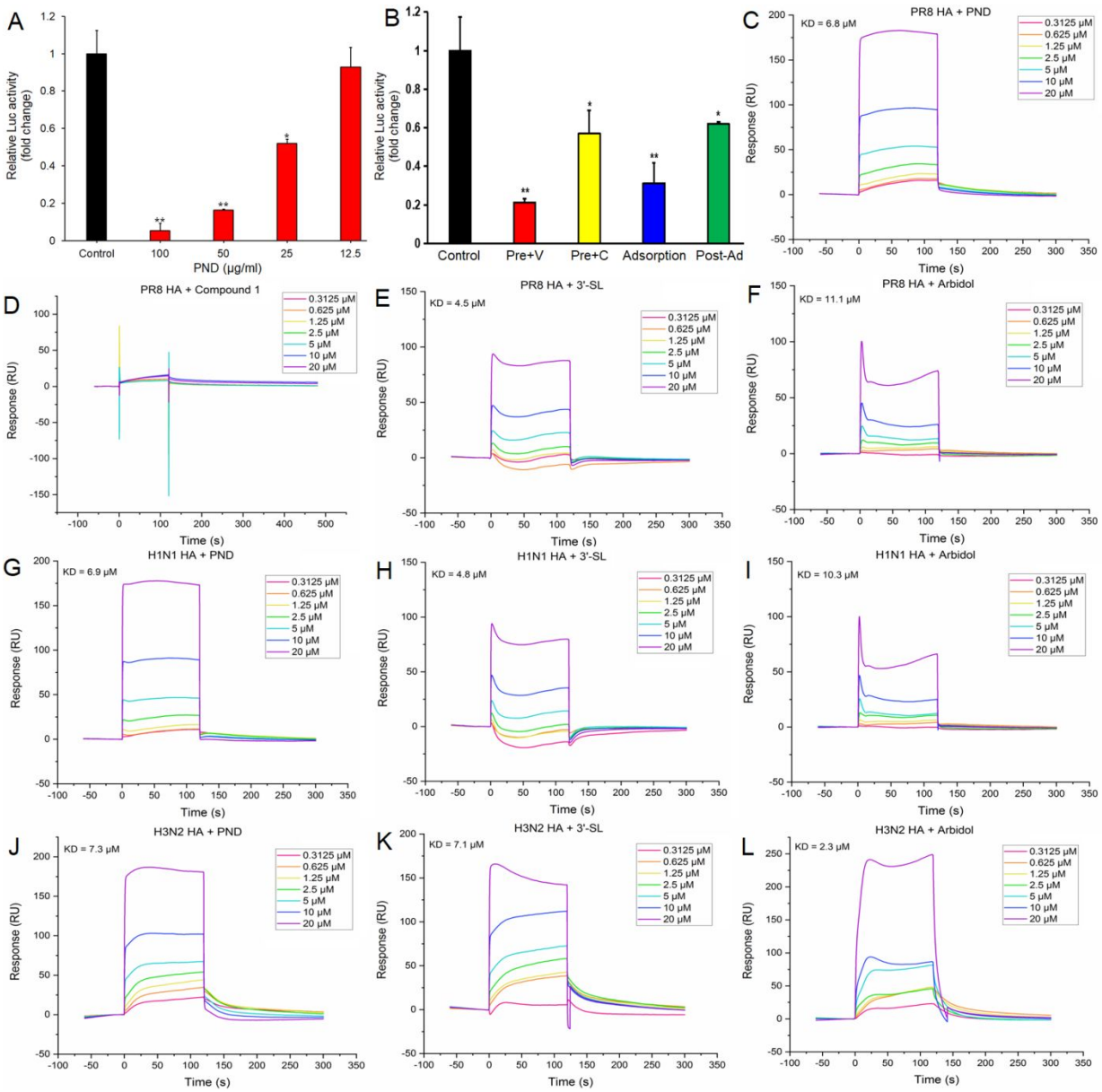

Figure 5. The direct interaction of compound PND with virus HA protein. (A) The H5N1 pseudovirus (H5N1-Luc) was pretreated with PND at 37 °C for 1 h before infection. At 48 h p.i., the amount of infected pseudovirus was determined by luciferase assay. (B) H5N1 pseudovirus (H5N1-Luc) infected MDCK cells were treated with 50 μg/ml of PND under four different treatment conditions. At 48 h p.i., the amount of infected pseudovirus was determined by luciferase assay. Values are means ± S.D. (n = 3). Significance: *P < 0.05, **P < 0.01 vs. virus control group. (C-F) To assess real-time binding of PND or control compounds to the PR8 HA protein on CM5 chips, PND, compound 1, 3'-SL, or arbidol (0.3125-20 μM) was flowed over the biosensor chip surface,

respectively. The sensorgram for binding interactions were recorded in real time and the changes in mass due to the binding response were recorded as resonance units (RU). (G-L) The SPR assay was also performed to evaluate the binding of PND, 3'-SL, or arbidol to the H1N1/Cal09 HA protein (G-I) or H3N2/Aichi HA protein (J-L), respectively. The KD values calculated by the BiacoreT200 SPR evaluation software were also shown.

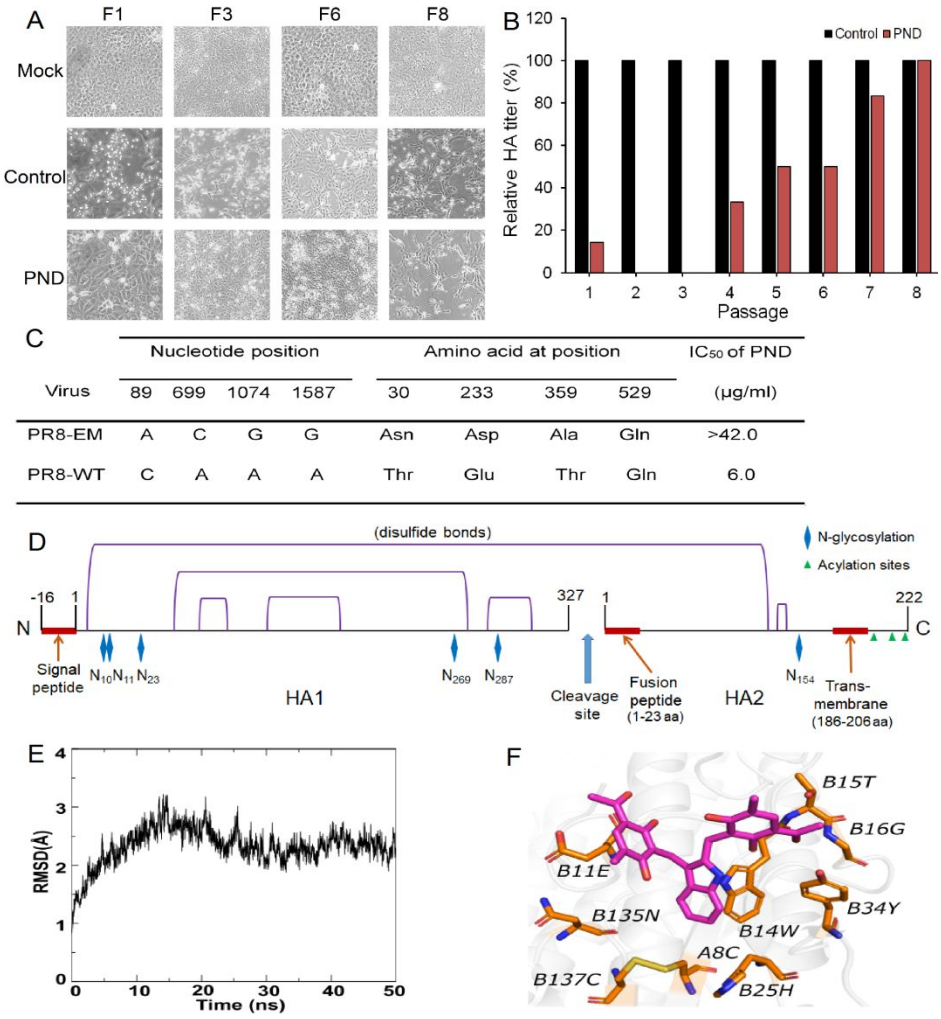

Figure 6. The potential binding sites of compound PND to virus HA protein. (A and B) Selection of escape mutant resistance to PND treatment at low dose (25 μg/ml) for continuous nine passages in MDCK cells. The microscopy observations of CPE at the 1st, 3th, 6th and 8th passage were shown in (A), and the relative yield of progeny virus by HA assay at each passage was calculated as percent of HA titers in PND-treated cultures compared with the untreated virus control group (B). (C) The nucleotide and amino acid changes of PR8 virus escape mutants resistant to PND treatment. (D) The structure of PR8 HA following cleavage into the HA1 and HA2 subunits. The mature HA contains 327 residues in the HA1 subunit and 222 residues in the HA2 subunit. (E) 50 ns MD simulations were performed to refine the binding mode of PND at the binding site of HA. (F) The binding mode of PND at the binding site of HA from molecular dynamics simulations. PND

(magenta) and residues of the binding site (orange) were shown in stick, and HA was shown in cartoon (light gray). Residues from A chain and B chain were labeled as “A” and “B”, respectively.

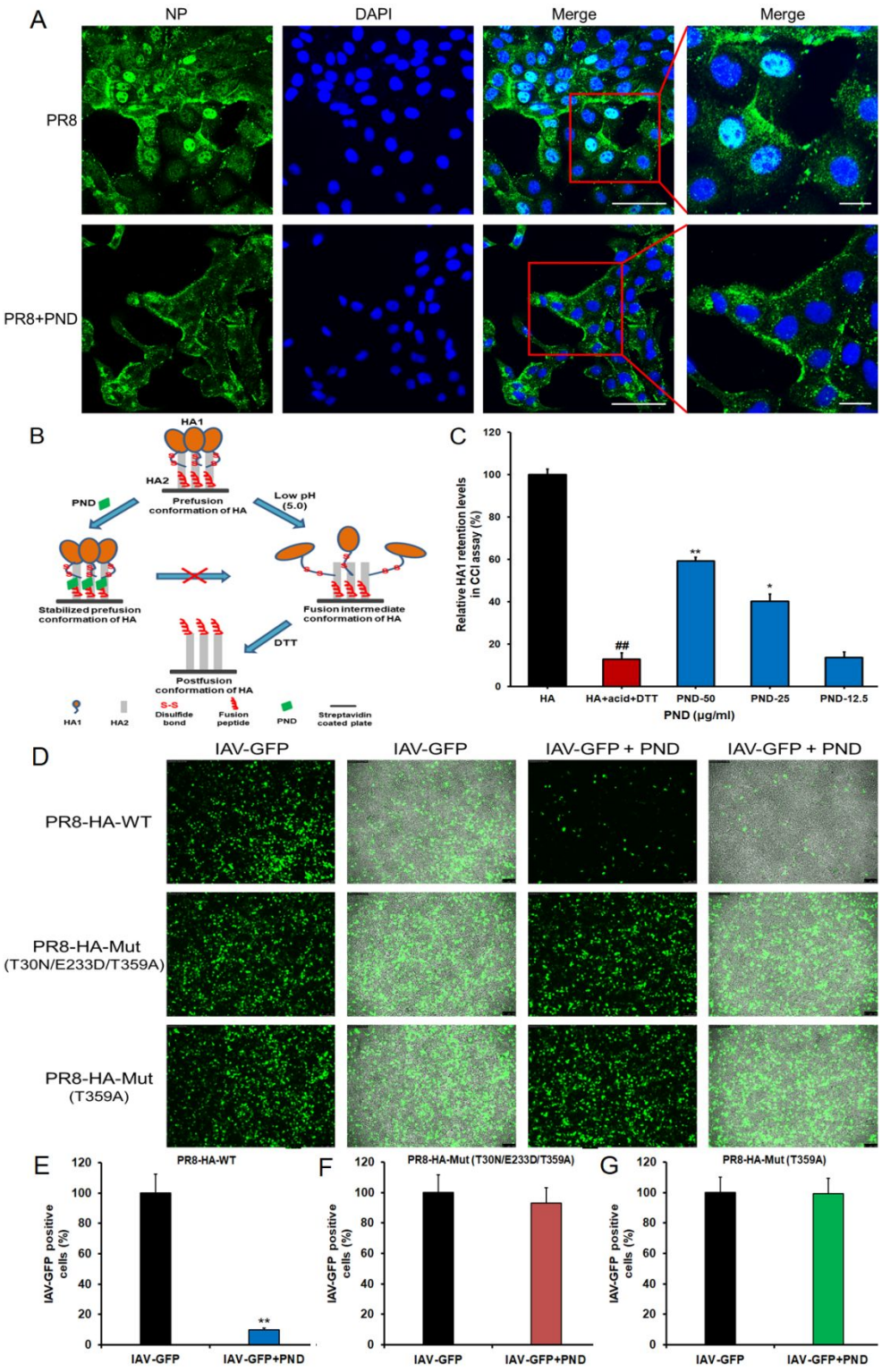

Figure 7. Mechanism of viral entry inhibition by PND. (A) PND blocked endocytosis of IAV. The localization of virus NP protein in PR8 virus infected A549 cells with or without PND treatment at 2 h p.i. was evaluated by using immunofluorescence assay. The scale bar represents 40 μm. An

enlarged view of part of one field (highlighted by the red rectangle) is also shown to indicate the detailed localization of NP. The scale bar represents 10 μm in this case. (B) Cartoon representation of the mechanism of conformational change inhibition by PND. HA trimeric is depicted as HA1, brown; HA2, gray; fusion peptide, red; and PND, green. (C) Conformational-change inhibition (CCI) assay showing that binding of PND (50, 25 μg/ml) to cleaved H1/PR8 HA blocks the low-pH-induced conformational change to increase the retention amount of HA1 subunit on HA proteins. The amount of HA1 subunit in control group without acidification (HA) was assigned a value of 100 and the data presented as mean ± S.D. (n = 3). Significance: ##P<0.01 vs. non-acidification control group (HA); *P<0.05, **P<0.01 vs. acidification control group (HA+acid+DTT). (D) The PR8/H1N1 pseudovirus (IAV-GFP) was prepared using plasmids encoding PR8 NA protein and the wild type (WT) HA protein or mutated HA proteins (T30N/E233D/T359A or T359A). Then these PR8 pseudoviruses (IAV-GFP) were pretreated with PND (50 *μ*g/ml) at 37 °C for 1 h before infection, respectively. At 48 h p.i., the amount of infected pseudovirus was observed using an inverted fluorescence microscope (DMI6000B; Leica, Germany) equipped with a cooled CCD camera. The scale bar represents 100 μm. (E-G) The average cell numbers of GFP positive cells in different images (n = 10) were measured by ImageJ (NIH) version 1.33u (USA) to evaluate the amount of infected PR8 pseudovirus (IAV-GFP) in 293FT cells. The average numbers of GFP positive cells for non-treated virus control cells (IAV-GFP) was assigned values of 100. Significance: **P < 0.01 vs. virus control group (IAV-GFP).

Table of Contents Graphic